

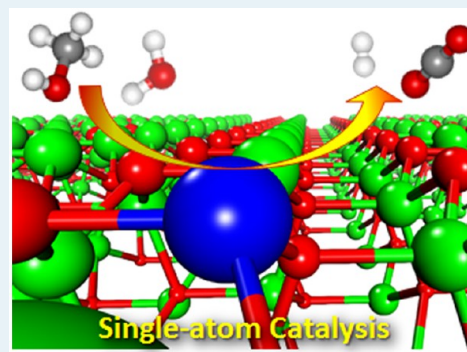
Catalysis by Supported Single Metal Atoms

Jingyue Liu*

Department of Physics, Arizona State University, Tempe, Arizona 85287, United States

ABSTRACT: The recent explosive growth in research on catalysis by supported single metal atoms proves the scientific interest in this new frontier of heterogeneous catalysis. A supported single-atom catalyst (SAC) contains only isolated individual atoms dispersed on, and/or coordinated with, the surface atoms of an appropriate support. SACs not only maximize the atom efficiency of expensive metals but also provide an alternative strategy to tune the activity and selectivity of a catalytic reaction. When single metal atoms are strongly anchored onto high-surface-area supports, SACs offer a great potential to significantly transform the field of heterogeneous catalysis, which has been critical to enabling many important technologies. In this Perspective, I discuss the most recent advances in preparing, characterizing, and catalytically testing SACs with a focus on correlating the structural perspective of the anchored single metal atoms to the observed catalytic performances. The grand challenge to successfully developing practical SACs is to find appropriate approaches to strongly anchor the single metal atoms and to keep them stable and functional during the desired catalytic reactions. I will highlight the recent advances to overcome this barrier to develop SACs for a variety of important catalytic transformations of molecules.

KEYWORDS: catalysis, single-atom, clusters, nanoparticles, noble metal, metal oxide, carbon, oxidation, reforming, hydrogenation, water–gas-shift, electron microscopy



1. INTRODUCTION

Metals constitute the most important catalytic systems for chemical transformation, energy conversion, and environmental remediation. Examples of using metals as catalysts include petroleum refining, fuel cells, abatement of emissions, and production of chemical intermediates, pharmaceuticals, and agrochemicals. Since most catalysis occurs on metal surfaces, any metal atoms that are not accessible by the reactant molecules are, to a large degree, wasted, and the fraction of these metal atoms should be minimized: Use of smaller metal particles with high surface/volume ratios has been the preferred choice. To prevent aggregation of metal nanoparticles (NPs) during a catalyst synthesis process or a catalytic reaction the metal NPs are usually dispersed, preferably anchored, onto high-surface-area and robust supports so the reactant molecules can reach as many surface atoms of the metal as possible. The dispersion (roughly defined as the number of surface atoms divided by the total number of atoms within a particle) is a reasonable descriptor for large metal NPs. For structurally sensitive reactions or for small metal NPs/clusters, however, the dispersion parameter becomes less meaningful for evaluating the catalytic properties of supported metals. The specific atomic configuration, the number of atoms within a metal cluster, and their interactions with the support surfaces become important in determining their catalytic performances.

Supported noble metal NPs are among the most important catalysts that enable many critical technologies, for example, energy production and environmental remediation.^{1–8} Noble metals are, however, expensive and of limited supply. Any development that reduces the consumption of precious metals,

increases their activity and selectivity, and/or improves their long-term stability is of essential importance. Enormous efforts have been devoted toward downsizing the metal NPs and improving their durability. Size reduction of metal NPs modifies their catalytic behavior via several channels: (1) surface effects, where the percentage of unsaturated coordination bonds of a metal NP increases;^{9–12} (2) quantum size effects, where confinement of electrons leads to increased energy levels and the widening of the Kubo gap (HOMO–LUMO gap);^{13–19} (3) metal–support interactions, where chemical bonding between metal and support becomes stronger and charge transfer may occur;^{20–25} and (4) cluster configurations, where the specific arrangement of atom positions and the number of atoms within a cluster can drastically change their physicochemical properties.^{10,26–30} As a consequence of these effects, small metal NPs or clusters usually show a distinct and complicated size effects on their reactivity.

The surface atoms of a metal NP possess dangling bonds which cost energy. Smaller NPs have a larger fraction of surface atoms, and thus, their average binding energy per atom is higher. The dispersion of metal NPs approximately scales with the inverse size, resulting in numerous properties which obey the same scaling law (e.g., the melting temperature of a metal NP). The edge and corner atoms on metal NPs have even lower coordination neighbors and therefore may tightly bind

Received: June 1, 2016

Revised: October 15, 2016

Published: October 18, 2016

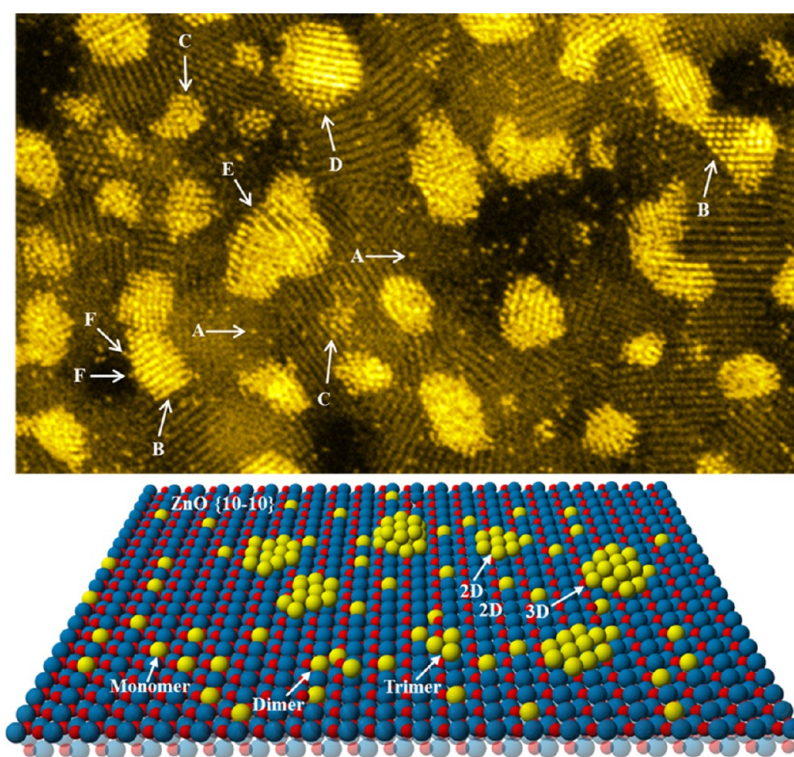


Figure 1. Top panel: Aberration-corrected HAADF-STEM image of a Pt/ZnO nanobelt model catalyst shows the presence of Pt single atoms (A), faceted Pt clusters (B), highly disordered Pt subnano clusters (C), reconstructed surface atoms of Pt nanoparticles (D), strained lattices of Pt (E), and highly unsaturated Pt atoms attached to the Pt nanocrystal (F); bottom panel: Schematic illustration of the various types of metal clusters, trimers, dimers, and monomers dispersed onto the ZnO {10-10} surface. During a catalytic reaction, all these various “sites” may contribute to the observed catalytic performance.

“foreign” atoms and molecules. Unlike surface atoms on large metal NPs, which behave like single-crystal surfaces, small metal clusters can be viewed as building up from single atoms, dimers, trimers, and so on, and they should behave more like atoms or molecules. When the number of atoms in a metal cluster becomes small, the “size” of the cluster is less well-defined and may become irrelevant for describing the cluster’s properties. Different isomers, for example, can possess very different physicochemical properties and can coexist over a range of temperatures. Many traditionally accepted concepts of thermodynamics, which originate from the statistical average of large number of events, may break down, especially for systems that consist of single isolated metal clusters with only a small number of atoms. The addition of a single “extra” or “foreign” atom to a small metal cluster of only a few atoms can reset the energy scale of the system because of quantum effects. Such discontinuities in total energy occur when a new shell at a higher energy level is needed to accommodate the additional atom. This quantum mechanical behavior rules out the existence of any simple scaling law related to the energy of the cluster. Ionization energies and electron affinities, which are important factors governing the adsorption of molecules, can fluctuate with the addition of a single atom to the metal cluster. Variations in the electronic structure of metal clusters affect their capability of forming bonds with other atoms or molecules as well as their redox reactions. Therefore, the catalytic activity and selectivity of small metal clusters should strongly depend on their number of atoms and specific atomic configurations.^{7,28}

Recent theoretical and experimental studies have demonstrated that subnanometer-sized clusters can have peculiar

properties. For example, negative heat capacities have been reported for isolated clusters.³¹ The local “temperature” of a cluster can fluctuate at a constant energy and is no longer well-defined. The electron affinities of isolated gold clusters, for example, can vary significantly with the number of atoms within the cluster: Odd-numbered cluster sizes possess a much higher electron affinity than that of the even-numbered cluster sizes.¹⁶ Such strong fluctuations with the total number of metal atoms in nanoclusters clearly affect their ability to donate or accept electrons and consequently their chemical reactivity. For example, the ionization potential of a Pt single atom is ~ 9.0 eV, becomes ~ 9.7 eV for a Pt dimer and approaches ~ 5.3 eV for bulk Pt metal.³² In the quantum regime of metal nanoclusters, addition or subtraction of even a single atom can drastically modify the cluster’s structural, electronic, optical, magnetic, and chemical properties. Furthermore, even for metal clusters with the same number of atoms their specific atomic configurations decide their physicochemical properties. The variations in the physicochemical, electronic, and catalytic properties, however, are not smooth but fluctuate significantly with the addition/subtraction of a single atom or the change of geometric configurations, a consequence of the nature of the transition from localized molecular orbitals to delocalized electronic band structures of solids. Such significant changes of ionization potential and electron affinity with cluster size and configuration can be effectively utilized for desirable catalytic properties. When metal clusters are dispersed on high-surface-area supports, their interactions with the support surfaces may play a paramount role in determining their catalytic properties. Subnanometer-sized metal clusters can have catalytic activity and/or selectivity different from,

sometimes better than, their larger NP counterparts.^{26–30,33–37} Supported metal clusters are configurationally complex and complicated.

Unless one utilizes very specialized synthesis techniques (which we will discuss later), it is extremely difficult, if not impossible, to routinely fabricate metal nanoclusters dispersed onto high-surface-area supports with exactly the same atomic configuration and number of atoms. In practical catalysts, for example, prepared via wet chemical methods, the supported metal catalysts usually consist of all types of shapes, configurations, and sizes of metal clusters or NPs. As an example, Figure 1 (top panel) shows an atomic resolution electron micrograph of Pt nanoclusters deposited, via a modified deposition–precipitation method, onto the surfaces of ZnO nanobelts. Many isolated single Pt atoms (indicated by the letter A), faceted clusters (indicated by the letter B), highly disordered or amorphous-like clusters (indicated by the letter C) as well as other types of clusters coexist on the support surface. Certain surface atoms of some larger Pt clusters (indicated by the letter D) seem to rearrange themselves into an atomic configuration that is far different from the termination of bulk Pt. Strained clusters (indicated by the letter E), either caused by the cluster–cluster interaction or due to the strong influence of the support surface, may possess unique electronic structures and catalytic properties. Highly under-coordinated Pt atoms attached to Pt facets (e.g., the atom indicated by the letter F) are frequently observed. Since the support surface is not a single crystal but consists of many randomly oriented ZnO nanocrystallites, some Pt clusters grew epitaxially on the ZnO surfaces while others did not. A schematic illustration of the various types of Pt metal clusters, trimers, dimers, and monomers on the ZnO {10–10} surfaces is presented in Figure 1 (bottom panel). During a catalytic reaction, all these various sites can contribute to the observed catalytic properties.

As unambiguously demonstrated by Figure 1, despite their small sizes, nanoclusters or subnanoclusters may contain multiple active centers which are not necessarily the most desirable active sites for specific catalytic processes, especially if these nanoclusters dynamically change their configurations during a catalytic reaction. To correlate the structure of these nanocluster catalysts with the observed catalytic performances is undoubtedly a formidable task. Clusters with controlled sizes but not necessarily controlled configurations can be fabricated by special physical or chemical methods.^{10,37} Ligand-protected metal clusters can provide well-defined sizes and atomic configurations.³⁹ The catalysis by these types of clusters are beyond the scope of this Perspective. Interested readers should consult the relevant reviews on this topic.^{10,37–39} The fundamental knowledge of supported metal nanoclusters is, however, relevant to the understanding of the catalytic properties of supported single metal atoms.

The most efficient approach to utilizing each and every metal atom in a supported metal catalyst is to downsize the metal nanoclusters to isolated individual atoms provided that the supported single metal atoms can yield desired catalytic properties. We adopt the recent definition of single-atom catalyst (SAC) as a supported metal catalyst which contains only isolated single metal atoms as the primary active centers.^{40,41} We want to emphasize that the abbreviation “SAC” always implies supported single atoms and that the catalytically active center of an SAC definitely consists of the isolated individual metal atom and may consist of their

immediate neighboring atoms of the support surface or surface functional groups. The chemical nature of the supported single metal atoms strongly depends on their interactions with the support surfaces and/or other associated surface species.

The SACs should not be confused with single site heterogeneous catalysts (SSHCs). By definition, a SSHC may consist of one or more atoms.⁴² A SSHC can consist of clusters of atoms as long as all the clusters catalytically behave the same way. If we assume, to the first order approximation, that all the isolated single metal atoms interact with the support surfaces or surface functional groups in the same manner then all the active sites of a SAC should be similar. Only in this special case, the SAC is equivalent to SSHC. As we will discuss later, however, for a practical high-surface-area catalyst support many types of surface structures and surface defects coexist and they interact with the adsorbed single metal atoms differently. Therefore, depending on the nature of the support surfaces and how the adsorbed individual metal atoms interact with the support surfaces and defects different types of catalytically active centers may coexist in a SAC even if only isolated single atoms are present in the SAC. In this Perspective, we will not discuss SSHCs since there are many excellent recent reviews on this topic.^{42–44}

The recent success in fabricating a variety of SACs for various catalytic reactions clearly and unambiguously demonstrated that heterogeneous catalysis on SACs is both fundamentally interesting and practically important.^{40,41,45–91} Furthermore, many theoretical (density functional theory (DFT)) calculations of different types of SACs have provided insights into the metal atom–support interactions and the catalytic cycles of SACs.^{40,68,69,92–99} It is interesting to note that within the last 5 years there seems to be an explosive growth in the study of SACs: More varieties of SACs have been fabricated; more catalytic reactions have been tested; and more DFT calculations have been conducted to understand the interaction processes (e.g., charge transfer) between single metal atoms and their supports and the catalytic cycles on single-atom based active centers. The surface science studies on single-crystal metals have provided deep insights into the fundamental knowledge of heterogeneous catalysis. The study of catalysis by supported single metal atoms is expected to provide valuable information on the nature of heterogeneous catalysis and to bridge heterogeneous and homogeneous catalysis.

In this Perspective, we primarily focus on discussing the synthesis, characterization, and the catalytic performance of isolated single metal atoms, especially noble metal atoms, dispersed onto open supports, such as metal oxides, or into porous carbon materials. We will specifically emphasize the importance of anchoring single metal atoms onto the support surfaces: Their physical location with respect to the support surface structure and the corresponding charge transfer due to strong metal–support interactions. Surface defects such as steps, kinks, corners, edges, surface cation and anion vacancies, color centers, impurities, and so on, may play a major role in anchoring the single metal atoms and subsequently determining their catalytic properties. Although zeolites and metal organic frameworks (MOFs) are an important class of support materials^{100–102} and many types of metal cations can be incorporated into these materials to significantly improve their catalytic performances, we will not discuss SACs related to these highly ordered microporous/mesoporous materials, which possess tremendous internal surface area. Interested

readers should consult the relevant research papers and reviews on this topic.^{54,100–108}

Density functional theory calculations have played a major role in understanding the specific catalytic reaction mechanisms of supported single metal atoms. Since only one metal atom is involved, the DFT calculations, compared to those for metal NPs and clusters, are significantly simplified. The appropriate modeling of the support surface, however, still poses a major challenge. The theoretical DFT calculations have proved to be extremely important for understanding the fundamental mechanisms of catalysis by supported single metal atoms. In this Perspective, however, we will not provide detailed discussions on the DFT calculations. Instead, we will use the results from the DFT calculations throughout this Perspective to illustrate our current understanding of the catalytic processes of supported single metal atoms. We briefly discuss the most recent applications of DFT calculations, in combination with characterization techniques, to probe the fundamental issues of SACs such as stability of the supported single metal atoms and the catalytic cycles of specific chemical reactions.

Since the research field of single-atom catalysis is in a burgeoning period of time, this Perspective will cover only selected examples, provide a basic understanding of how SACs work, and, based on the author's own point of view, discuss the great opportunity and challenges in developing practical SACs. Several reviews on SACs and atomically dispersed supported metal catalysts have been published in the past few years. The readers should consult the relevant reviews by Flytzani-Stephanopoulos and Gates,⁵⁴ Yang et al.,⁴¹ Flytzani-Stephanopoulos,⁶⁷ and Narula and Moses-DeBusk.¹⁰⁹ This Perspective is not intended to be an exhaustive review of the field; it only provides a snapshot of a rapidly growing research field of heterogeneous catalysis. Compared to our earlier review,⁴¹ this Perspective updates the catalysis community with respect to the variety of catalytic reactions conducted on SACs, new approaches to anchor single metal atoms, and fundamental understanding of the catalytic mechanisms of SACs. This Perspective is also intended to clarify some misconceptions or confusions about SACs, to summarize the wide applications of SACs to various catalytic reactions, and to provide a future perspective on this rapidly advancing research field.

2. UNIQUE FEATURES OF SINGLE-ATOM CATALYSTS

Since a SAC consists of only isolated single metal atoms dispersed onto the surfaces of a support material the dispersion of a metal SAC, by definition, is always 100%. Such catalysts possess unique properties different from those of the conventional supported metal NP catalysts. We discuss a few of these unique features below.

2.1. Definitions and Classifications. There seems to be some confusion about the use of different terms to describe a few related but different types of supported metal catalysts. In this Perspective, we define the following terms so there will be no confusion or ambiguity when we use them. **Figure 2** schematically illustrates the differences among the four types of catalysts that we discuss below.

Single-Site Heterogeneous Catalyst (SSHC).⁴² The “single site” may consist of one or more atoms. Such single sites are spatially isolated from one another, and there is no spectroscopic or other cross-talk between such sites. Each site has the same energy of interaction between it and a reactant as every other single site; and each such site is structurally well-

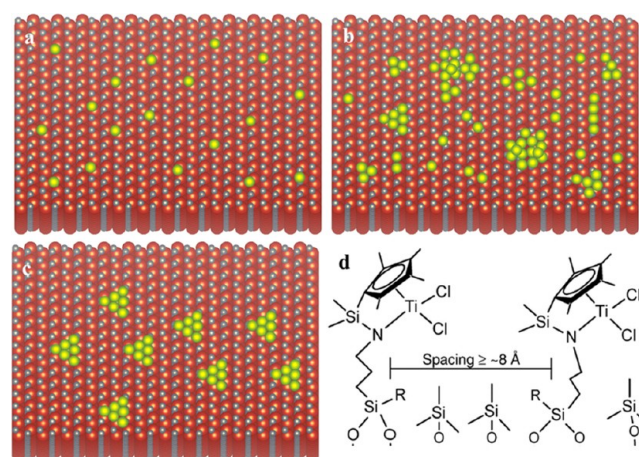


Figure 2. Schematic illustrations of (a) a supported single metal-atom catalyst (SAC), (b) an atomically dispersed supported metal catalyst (ADSMC), (c) an extreme example of a single site heterogeneous catalyst (SSHHC), and (d) a site-isolated heterogeneous catalyst (SIHC). Panel d is adapted from ref 110.

characterized, just as the single sites in homogeneous molecular catalysts are.

Single-Atom Catalyst (SAC).^{40,41} The catalyst contains only isolated single atoms dispersed on a support. There should be no spatial ordering or any other types of appreciable interactions among the isolated individual atoms. The active sites generally consist of the single metal atoms as well as the immediate neighboring atoms of the support surface or other functional species. The catalytic property of the individual active sites can be similar or different depending on the interaction between the single metal atom and its neighboring atoms. When the catalytic behavior of all the individual atoms in a SAC is similar or the same, then the SAC can be considered to be an SSHC as well.

Atomically Dispersed Supported Metal Catalyst (ADSMC). The dispersion of the supported metal is considered to be 100%. The metal, however, can be in the form of two-dimensional rafts, small clusters, trimers, dimers, monomers, and so on. The defining parameter is 100% dispersion of the metal. SAC can be considered as a subset of ADSMC. The structure and catalytic performance of an SAC are much better defined than those of an ADSMC.

Site-Isolated Heterogeneous Catalyst (SIHC). This term generally refers to a heterogeneous catalyst that contains spatially well-separated organometallic complexes. The organometallic complexes possess well-defined structures, and they can be anchored to the support surfaces by ligands. A typical example is to graft organometallic complexes on a silica surface.^{110–112} The active sites of SIHCs may contain many metal atoms and the metals do not have to be atomically dispersed. The unique feature of a SIHC is that the active center is protected by ligands, and all the active centers behave in the same manner. An SIHC with only one type of active center can be considered to be an SSHC and in the reported literature SIHC and SSHC frequently used interchangeably.

Generally speaking, SSHC can usually be realized with ordered microporous/mesoporous supports such as zeolites,⁴² whereas functionalization and immobilization of functional groups are critical to developing SIHCs.^{110–112} SACs in general are not SSHCs because the interactions of isolated metal atoms with the support strongly depend on the heterogeneous nature

of the surface structures and defects of the support materials. When single metal atoms are incorporated into well-defined and highly ordered mesoporous structures or when they only interact with structurally well-defined functional groups on the support surfaces, they can be considered as SSHCs. For example, Flytzani-Stephanopoulos reported that for water–gas-shift (WGS) reaction the intrinsic activity of the Au–O_x(OH)–S site (where S represents support)⁶⁸ and catalytically similar single-atom-centric Pt sites formed by binding to Na ions through –O ligands⁸¹ is the same for a variety of support materials. In these special cases, the SACs catalytically behave like SSHCs.

2.2. Additive Nature of SACs. An effective assessment of the catalytic performance of a SAC is to measure its specific activity per weight or the turnover frequency (TOF) per atom. Since a SAC, by definition, contains only isolated single atoms, the TOF and the specific activity per metal atom (site) should be, ideally, constant regardless of the loading levels of the metal. For a specific catalytic reaction, the total activity of a SAC should have a linear relationship with the metal loading level. When the number density of single metal atoms is high metal clusters may form, and such a simple linear relationship may not apply any more.⁴¹ From this point of view, high-surface-area supports are highly desirable for developing high metal loading SACs. As we will discuss later, the specific location of the single metal atoms on the support surface influences their strength of interaction with the support, which in turn affect their catalytic performances. In general, the structure and chemical reactivity of the support surfaces become important for supported metal clusters, especially for single metal atoms.

2.3. Ubiquitousness of Single Atoms in Supported Metal Catalysts. Since thermodynamically metal NPs or clusters are not stable, they grow during postsynthesis treatments or catalytic reactions, especially at high temperatures. The major sintering mechanism is generally the Oswald ripening process: Metal atoms emit from smaller NPs to be absorbed by larger NPs (Figure 3). Since this process ubiquitously occurs during almost all catalytic reactions on supported metal NP catalysts, one can visualize that at any moment during a catalytic reaction, single metal atoms are present on the support surfaces. It is not difficult to picture that many industrially important catalytic reactions on supported

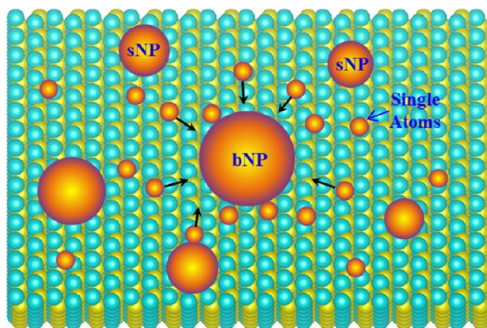


Figure 3. Schematic diagram illustrates the presence of single atoms on a support surface during Oswald ripening process. Particle sintering by the Oswald ripening process occurs in most supported metal catalysts, especially at high reaction temperatures. During the sintering process, smaller metal particles disappear and larger metal particles grow bigger. This process is accomplished by diffusion of single metal atoms on the support surface. sNP: small metal nanoparticles; bNP: big metal nanoparticles.

metal catalysts may occur on these “mobile” single metal atoms. Therefore, the contribution to the observed catalytic performances from single metal atoms should be carefully evaluated, even for commercial catalysts. For certain reactions, as will be demonstrated in this Perspective, the supported single metal atoms may contribute significantly to the observed activity or may adversely or beneficially influence the selectivity. In fact, it is extremely difficult, if not impossible, to maintain a supported metal catalyst that does not contain any single metal atoms during a catalytic reaction.

3. SYNTHESIS OF SINGLE-ATOM CATALYSTS

A prerequisite for studying the catalytic properties of SACs is to disperse isolated single metal atoms onto the appropriate support surfaces. Fabrication of SACs, however, has been challenging because of the tendency of aggregation of metal atoms either during the synthesis processes or the subsequent treatments. First of all, one has to find a way to transfer metal atom species to the support surfaces. For example, unless the single metal atoms or metal complexes have a strong affinity for the surfaces of the support materials during a wet chemistry synthesis they will form clusters or NPs either in the solution or on the supports. We discuss below a few methods that have been utilized to prepare SACs. Table 1 provides a partial list of the synthesis methods for producing supported metal SACs.

3.1. Mass-Selected Soft-Landing Method. The mass-selected soft-landing method has been proved to be extremely powerful for synthesizing metal clusters with precisely controlled number of atoms.^{28,37} This technique can be used to prepare SACs as well. Because it is a physical deposition method, any types of flat supports can be used. Furthermore, any metal clusters with precisely defined number of atoms can be produced and “soft-landed” onto the surface of the desired substrates. This technique provides excellent model catalysts for fundamental studies, on the atomic level, of metal–support interactions and the effects of metal cluster size on their catalytic performances. The disadvantages of such a method include cost and low yield. Furthermore, such a deposition method is not suitable for high-surface-area supports or mesoporous support materials and is clearly not appropriate for practical industrial applications.

3.2. Metal Leaching Method. This method derives from the recovery of Au from Au-containing ores and has been used by Flytzani-Stephanopoulos’ group to produce metal cations supported on metal oxides.^{46,109} Typically, a conventional supported metal catalyst is first prepared and then the catalyst is immersed into a dilute aqueous solution of 2% NaCN under O₂ gas flushing at room temperature. NaOH is added to maintain the solution at a high pH value. The leaching process is fast and selective. The solution treatment only leaches the metal NPs but keeps the metal cations intact. The final amount of the metal ions left on the oxides can then be determined by metal analysis techniques. Such an approach may be applied to certain selected metals and supports. Environmental concerns, however, may limit this method for large-scale applications.

3.3. Wet-Chemistry Method. Generally speaking, most of the wet-chemistry methods^{114,115} can be employed to synthesize supported metal SACs. In the wet-chemistry approach, because the precursor materials already contain single atom metal species, the objective is to anchor the metal complexes onto the supports through a chemical reaction while avoid their aggregation during the synthesis and post-treatment processes. Experimentally, anchoring mononuclear organo-

Table 1. Partial List of Synthesis Methods for Producing Single-Atom Catalysts

method	comments on support materials	examples	references
mass-selected soft-landing	any substrate but not high-surface-area supports	Rh/Pd/Pt/Au on MgO, Pt/Au on Si, Au/Ag/Cu/Co on Al ₂ O ₃	28, 37
metal leaching by cyanide salt	not for oxides that cannot stand high pH solution	Au/Pt/Pd on CeO ₂ , Au/FeO _x , Au/Pt/TiO ₂ , Pt/SiO ₂ , Pt/MCM-41	46, 67, 79, 113
coprecipitation	any catalyst supports	Pt/FeO _x , Au/FeO _x , Ir/FeO _x	40, 60, 65
deposition–precipitation	any support materials that do not dissolve at the required solution pH	Au/FeO _x , Pd/Au/Pt/Rh on ZnO, Au/Pt/Pd on CeO ₂	68, 72, 82, 85
strong electrostatic adsorption	any support materials that do not dissolve at the required solution pH	Pt/C, Pt/Au/Pd on Al ₂ O ₃ , Au/Pt/Pd on FeO _x , Pt/Pd/Au on ZnO	118–120
atomic layer deposition	catalyst support materials	Pt/C, Pt/SiO ₂ , Pt/TiO ₂ , Pt/ZrO ₂ , Pt/Al ₂ O ₃	62, 123, 146
organometallic complex	catalyst support materials	Ir/Rh/Ru/Pt/Os clusters on MgO/SiO ₂ /Al ₂ O ₃ /zeolites	10, 107, 124, 125
combustion synthesis	mostly oxides	Pt/Rh/Pd/Au/Ag/Cu doped into CeO ₂ , TiO ₂ , Al ₂ O ₃ , and ZnO	131, 132
pyrolysis synthesis	mostly carbon based supports	Pd/Pt on C ₃ N ₄ , Pt/Pd/Nb/Co/Fe on N-doped carbon	77, 78, 164
high-temperature vapor transport	selected oxides	Pt/CeO ₂ , Ag/Sb on ZnO	133
cluster synthesis	selected materials	[AuFeO ₃] ⁻ , [VAlO ₄] ⁺ , [PtZnH ₅] ⁻ , [AuCeO ₂] ⁺ , Au _x (TiO ₂) _y O _z ⁻ , AuAl ₃ O ₅ ⁺ , PtAl ₂ O ₄ ⁻	127–130
ion implantation	not for internal surfaces or high-surface-area supports	N-doped C/SiC	126

metallic complexes onto supports can be achieved by coordinating the ligands of the complexes to the surface groups of the support materials.^{10,42,47,55,116} In many catalytic processes, more accessible metal active sites are needed, which requires various types of pretreatment of the precursor materials to remove the undesirable or poisonous ligands. As a result, the isolated single metal atom species may aggregate to form larger clusters or NPs. Strong metal–support interaction is key to preventing aggregation of isolated single atoms. In practice, one can easily produce supported metal SACs by reducing the amount of metal loading to an extremely low level.

The most common wet-chemistry approach to preparing dispersed metal catalysts requires a combination of sequential processes: (1) introduction of the metal precursor on the support by impregnation/ion-exchange, coprecipitation, or deposition precipitation, (2) drying and calcination, and (3) reduction or activation. The advantages of the wet-chemistry approach is that this method does not require specialized equipment and can be routinely practiced in any wet chemistry lab. Furthermore, this is the preferred method for commercial production of supported metal catalysts.

3.3.1. Impregnation Method. The dry/incipient wetness method is simple and does not waste costly reagents, but it may be difficult to produce uniformly distributed single metal atoms. The wet/soaking process depends on the capability of the support surface to adsorb the precursor complexes, and therefore, precursor–support interaction becomes critical. The final amount of metal loading and dispersion strongly depends on the nature of the anchoring sites on the support surfaces.

When suspended in an aqueous solution many oxide supports (e.g., MgO, Al₂O₃, SiO₂, TiO₂, etc.) polarize and carry surface charge, which is controlled by the pH of the solution. In an acidic solution, the adsorption surface site (M–OH) is positively charged and covered by anions, whereas in a basic solution, the adsorption surface site (M–OH) is negatively charged and covered by cations. According to the Brunelle adsorption model,¹¹⁷ the key parameters that controls the metal dispersion include (a) the type and concentration of the metal precursor, (b) the pH of the aqueous solution, and (c) the type of the support and its surface functional groups. Complex ions of various types of metal precursors and the use

of nonaqueous impregnating solutions can tune the adsorption behavior for specific purposes. For example, chlorometallic ions can form aquo-complexes, and hydrolysis can occur, complicating the metal adsorption behavior.

The wet impregnation method may not be appropriate for synthesizing high metal loading catalysts but is suitable for preparing SACs on open supports, especially individually separable nanostructures. By controlling the types of metal precursors and their interactions with the support anchoring sites, localization of the desired single metal atoms can be primarily controlled by the wet impregnation step. The subsequent appropriate calcination processes can be utilized to further disperse the metal species to form isolated single metal atoms anchored onto the support surfaces.

3.3.2. Coprecipitation Method. By the nature of the coprecipitation process, in principle, a uniform distribution, on a molecular level, of the different active species can be obtained. The characteristics of the final catalysts, however, depend on many parameters including the order and the speed of the addition of the component solutions, the sizes of the droplets, efficient mixing, the temperature of the base solution, the pH value, the aging time, and so on. Noble metal SACs have been successfully synthesized by coprecipitation.^{40,60,65} A major issue for this approach to synthesizing metal SACs is that some metal atoms can be buried at the interfacial regions of the support agglomerates and within the bulk of the support crystallites. These buried single atoms are thus not accessible by the reactant molecules, significantly compromising the effectiveness and efficiency of the SACs.

3.3.3. Deposition–Precipitation Method. This method involves the precipitation of a metal hydroxide or carbonate on the supports via the reaction of a base with metal salt complexes. A critical concern is the formation of small metal (hydroxide) clusters or NPs in the solution phase before the metal ion complexes can be adsorbed onto the supports. Although the deposition–precipitation approach may not work well for high levels of metal loading this method is extremely powerful for producing uniformly distributed single metal atoms with very low levels of metal loading.^{68,72,82,85} Engineering of anchoring sites on the support surfaces and control of the interaction between the metal-containing solution and support surfaces are essential to synthesizing high-metal-loading SACs.

3.3.4. Strong Electrostatic Adsorption. Strong adsorption of metal ion complexes onto the support surfaces is critical to producing high-quality metal SACs, especially noble-metal-based SACs. Brunelle postulated that the adsorption of noble metal complexes onto most oxides is essentially Coulombic in nature.¹¹⁷ Oxide surfaces are usually covered with hydroxyl groups, and when the oxides are in an aqueous solution, they become positively charged below the PZC (point of zero charge) of the oxides or negatively charged above the PZC. Under these conditions, the metal ion complexes deposit onto the support surfaces via strong electrostatic adsorption (SEA).^{118–120} When the metal ion complexes are strongly anchored onto the support surfaces to form a monolayer and the subsequent treatments to remove the undesired ligands do not destabilize the metal atoms, a maximum loading of single metal atoms can be realized. The spatial distribution of functional groups on the supports is, however, usually heterogeneous, and the presence of various types of surface defects significantly influences the adsorption behavior of the metal complexes. Furthermore, the solution pH usually shifts with adsorption time and consequently affects the quality of the final SACs. Functionalization of support surfaces with strong anchoring species is key to successfully developing stable SACs.

3.4. Atomic Layer Deposition Method. Atomic layer deposition (ALD), originated from the need of making atomic layer epitaxy to fabricate effective electroluminescent display¹²¹ and to make metal oxide thin films,¹²² has been adapted to fabricate catalysts with atomically precise design and control.¹²³ This technique has been utilized to synthesize single metal atoms on graphene or other types of supports.⁶² In the ALD process, the selected support material is alternately exposed to the pulsing vapors of different reactive precursors. The key character of the ALD method is its self-limiting manner to deposit materials in an atomic layer-by-layer fashion.

Since one can precisely control the growth of different layers of materials to form composites with various types of morphologies the ALD technique can provide desired model catalysts for studying fundamental mechanisms of catalytic processes and the effects of particle size, nature of the support surfaces, overlayers on metal or alloy NPs, and so on. It is expected that broad applications of ALD and its associated characterization techniques can shed more light on the catalytic properties of metal nanoclusters or even single metal atoms. Because of the scalability issue and cost, it may not be possible, at least in its present format, to use this technique to produce catalysts for commercial applications. As a method for preparing better-controlled nanocluster catalysts for fundamental study, it is expected that ALD can become a powerful tool for studying the synthesis-structure-performance relationships of supported metal catalysts including supported metal SACs.

3.5. Organometallic Complexes Approach. The use of molecular complexes such as organometallic complexes clearly offers advantages in studying the catalytic behavior of supported metal species because these molecular complexes possess well-defined structures or ligands.^{10,107,124,125} The precursors are organometallic compounds that coordinatively react with support surfaces. Typical precursor ligands can react with supports to make structurally well-defined metal–oxygen bonds. The supported metal catalysts, including SACs, typically contain reactive ligands (e.g., alkyls, allyls, or carbonyls) bonded with oxygen atoms or OH groups on oxides or zeolites. In some cases, the OH groups on an oxide surface behave as ligands to a metal center of an organometallic

complex, resulting in anchoring of such complexes. This preparation method utilizes the structural uniformity of molecular complexes to fabricate site-isolated supported metal catalysts with precise control of the number of metal atoms and probably the structure of the anchored complexes as well. To keep the original character of the molecular complexes, however, requires the presence of the ligands and the strong interaction of the ligands with the support functional groups. This method may provide desired model catalysts for fundamental studies of the catalytic behavior of anchored organometallic complexes. Unless the metal ligands are removed, which may result in the degradation of the well-defined composition, structure, and configuration, the catalytic behavior of the SACs, synthesized via the organometallic complex approach, may be very different from that of the SACs that are synthesized through traditional wet-chemistry methods which are industrially viable.

3.6. Other Synthesis Methods. Ion Implantation. Supported metal SACs can be synthesized via other approaches as long as isolated single metal atoms act as catalytically active centers. When two-dimensional materials such as graphene, oxide sheets, and dichalcogenides are used as support materials the low-energy ion implantation method can be used to produce highly doped materials.¹²⁶ Such a method can be adapted to fabricate model metal or even nonmetal SACs for investigating the catalytic behavior of highly doped two-dimensional catalytic materials.

Doped Metal Oxide Clusters. Single-atom doped metal oxide clusters have demonstrated various types of catalytic reactions in the gas phase.^{127–130} In this case, the doped clusters can be fabricated by a special system that consists of laser ablation and supersonic expansion cluster source coupled with a fast flow reactor. Such gas-phase metal oxide cluster studies under isolated, controlled, and reproducible conditions can provide mechanistic insights into the working mechanisms of supported metal catalysts and supported metal SACs.

Combustion Synthesis of Doped Metal Oxide SACs. Combustion synthesis (CS) or self-propagating high-temperature synthesis (SHS) is an effective, low-cost method for production of various industrially useful materials, especially oxides. Combustion synthesis method has been used to produce noble-metal-doped metal oxide nanocrystallites.^{131,132} The noble metals exist as positively charged ions throughout the metal oxide nanocrystallites. Such catalysts can be considered as SACs as well, and structurally they are substitutionally cation doped metal oxides. The disadvantages of such a method include the presence of large amount of (noble) metal atoms in the interior regions of the metal oxides, the reduced control of the metal–support interactions, and other factors.

Pyrolysis Synthesis of Carbon-Based M_1 SACs. This method is generally used for preparing carbon-based catalysts. N-doped porous carbons are usually the preferred choice of supports. After metal precursors are incorporated into the porous carbon materials, the whole system is put into inert gas for high-temperature treatment. Noble metal or non-noble single metal atoms can be incorporated into the porous carbons and be stabilized by strong binding to N or other functional groups.^{77,78} High-metal-loading SACs can be produced via this method with high-surface-area carbon supports.

High-Temperature Vapor Transport Method. Under oxidizing conditions and at high temperatures, certain metals such as Pt can be emitted as volatile (PtO₂) molecules. If these

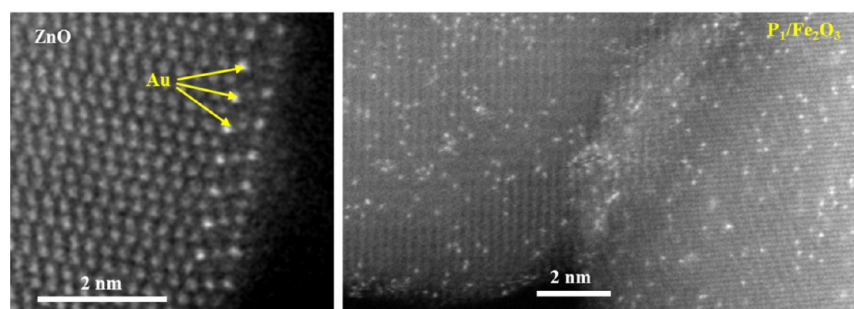


Figure 4. Aberration-corrected HAADF-STEM images of a ZnO nanowire dispersed with individual Au atoms (left panel) and Pt atoms in a highly loaded Pt₁/Fe₂O₃ SAC (right panel). The “bright dots” in the right panel image represent Pt single atoms; the contrast of the Pt single atoms depends on the location and stability (under electron beam irradiation) of the Pt atoms.

molecules are captured by the surfaces of another support which stabilize the metal-containing molecules then single metal atoms can be uniformly dispersed onto the support surfaces to produce a SAC. This method has recently been used to produce thermally stable Pt₁/CeO₂ SACs.¹³³ The SAC was tested for CO oxidation and demonstrated sintering-resistant behavior at high temperatures. The use of CeO₂ nanocrystals as the trap for the PtO₂ molecules is critical to the successful synthesis of the Pt₁/CeO₂ SACs. This technique may be applicable to synthesizing other types of stable SACs.

4. CHARACTERIZATION OF SINGLE-ATOM CATALYSTS

By definition, SACs only contain isolated single atoms that act as the centers of the catalytically active sites. Therefore, confirming the existence of only isolated single metal atoms and determining their spatial distribution become most critical to developing SACs. The most convincing and intuitive approach is to directly image the single metal atoms dispersed on high-surface-area supports. Both the scanning tunneling microscopy (STM)⁵² and the aberration-corrected electron microscopy (ACEM) techniques^{25,40,55} can provide such direct observation of single metal atoms. X-ray absorption near edge spectroscopy (XANES) and extended X-ray absorption fine structure (EXAFS) spectroscopy techniques can provide information about the dispersion of the metal clusters or even single atoms, the nature of the neighboring atomic species, and their oxidation states.^{10,42} By using appropriate probe molecules (e.g., carbon monoxide, ammonia, pyridine, etc.), infrared (IR) spectroscopy can be used to evaluate the existence of single metal atoms and, to a certain degree, to quantify the percentage of the dispersed single metal atoms in a supported metal catalyst.^{134,135} The spectroscopy techniques can be conducted *in situ* or *operando*, providing useful information on the nature of the working catalysts.

4.1. Integrated Electron Microscopy Approach. The integrated electron microscopy approach to characterizing supported metal catalysts, especially supported noble metal catalysts, has proven to be valuable to reliably evaluate the quality of supported metal catalysts. This method is extremely powerful for confirming the existence of only single metal atoms without the presence of any metal clusters or NPs, identifying the location of the single metal atoms with respect to the surface structure of the support, and determining the spatial distribution of the single metal atoms.^{25,40,60–66,88–85} Such a technique is indispensable to developing and optimizing synthesis protocols that reliably produce metal SACs. Figure 4 shows aberration-corrected high-angle annular dark-field

scanning transmission electron microscopy (HAADF-STEM) images of Au single atoms decorated on the {10–10} nanofacet of a ZnO nanowire (Figure 4a) and Pt atoms in a Pt₁/Fe₂O₃ SAC (Figure 4b). The individual Au and Pt atoms (bright dots) are clearly visible with excellent image contrast. The successful application of aberration-corrected HAADF-STEM in the past few years has provided invaluable information on the nature of supported metal SACs and in optimizing synthesis protocols to fabricate supported metal SACs.^{25,40,60–66,88–85}

Compositional analyses of individual metal atoms is still not routinely available by energy-dispersive X-ray spectroscopy (EDS) and electron energy loss spectroscopy (EELS). The electron-beam-induced effects and the detection sensitivity pose a serious obstacle to routinely identifying the nature of individual atoms dispersed on high-surface-area supports. When the single metal atoms are embedded into the surfaces of two-dimensional support materials or are located in the interior regions of a support both the EELS and EDS techniques can be used to identify the atomic species of the individual atoms and, in favorable cases, to provide information on the oxidation state of the probed atoms.^{136–138}

4.2. Spectroscopy Techniques. EXAFS and XANES. The XANES and EXAFS techniques have been extensively used to characterize the nature of supported metal NPs or clusters.^{10,42,139,140} Gates' group has used these techniques in the past decades to characterize supported metal clusters and molecular complexes with precisely controlled number of atoms and structures.^{10,139} The ability of EXAFS spectroscopy to determine the metal–metal coordination numbers can be effectively utilized to evaluate if SACs have been successfully fabricated. By definition, the metal–metal bonds of the active species should be absent in the EXAFS spectra of SACs. Therefore, if the EXAFS data does not contain any signal on the metal–metal bonding, by inference, one can conclude that only single metal atoms are present in the catalyst. The EXAFS technique was successfully applied to evaluating the nature of Pt₁/FeO_x catalysts.^{40,50,65} Table 2 shows the EXAFS data fitting results of a series of Pt/FeO_x catalysts with various levels of Pt loading.⁶⁵ As clearly shown in Table 2, the Pt–Pt coordination number *N* decreases with the decrease of Pt loading from 4.3 wt % to 0.75 wt %. When the Pt loading level was decreased to 0.08 wt % and the catalyst was reduced at 200 °C the EXAFS data did not show any Pt–Pt bonding (last row in Table 2). The Pt–O at 2.01 Å with *N* = 3.9 and the Pt–Fe at 3.05 Å with *N* = 3.3 were detected. The much longer distance of Pt–Fe coordination (denoted as Pt–Fe_{long}) than that of Pt–Fe alloy (2.54 Å) suggests that the Pt may not directly coordinate with Fe but via a bridging O.⁶⁵ When the reduction temperature was

Table 2. EXAFS Data Fitting Results of Pt/FeO_x Catalysts with Different Pt Loadings (adapted from ref 65)^a

samples	shell	N	R (Å)	$\sigma^2 \times 10^2$ (Å ²)	ΔE_0 (eV)
Pt foil	Pt–Pt	12.0	2.76	0.41	6.1
PtO ₂	Pt–O	6.0	2.00	0.41	7.2
	Pt–Pt	6.0	3.08	0.99	2.1
4.30%Pt/FeO _x -R250	Pt–O	0.6	1.95	0.30	−3.5
	Pt–Fe	1.5	2.52	0.82	−3.5
	Pt–Pt	2.3	2.62	0.82	−3.5
2.73%Pt/FeO _x -R250	Pt–O	1.4	2.00	0.30	6.4
	Pt–Fe	0.8	2.54	0.54	6.4
	Pt–Pt	1.4	2.68	0.54	6.4
0.75%Pt/FeO _x -R250	Pt–O	1.8	2.00	0.17	5.1
	Pt–Fe	0.9	2.52	0.36	5.1
	Pt–Pt	0.5	2.73	0.36	5.1
0.08%Pt/FeO _x -R250	Pt–O	2.0	2.01	0.26	8.4
	Pt–Fe	1.0	2.55	0.47	8.4
	Pt–Pt _{long}	1.1	2.99	0.47	8.4
	Pt–Fe _{long}	0.8	3.08	0.47	8.4
0.08%Pt/FeO _x -R200	Pt–O	3.9	2.01	0.11	7.4
	Pt–Fe _{long}	3.3	3.05	1.09	7.4

^aN: the coordination number for the absorber-backscatterer pair; R: the average absorber–backscatterer distance; σ^2 : the Debye–Waller factor; ΔE_0 : the inner potential correction. The accuracies of the above parameters were estimated as N ($\pm 20\%$); R ($\pm 1\%$); σ^2 ($\pm 20\%$); ΔE_0 ($\pm 20\%$). The data range used for data fitting in k-space (Δk) and R-space (ΔR) are 3.0–10.7 Å^{−1} and 1.2–3.5 Å, respectively.

increased to 250 °C, however, the EXAFS data did show the formation of Pt–Pt bonding but with a distance much longer than that of Pt–Pt distance in bulk Pt. This suggests that a certain degree of aggregation of Pt atoms occurred during the 250 °C reduction treatment, but the Pt atoms did not form small crystals yet. This example clearly demonstrates the power of EXAFS in characterizing the nature of supported metal cluster and NP catalysts as well as SACs.

Figure 5a shows the XANES spectra on the same set of Pt/FeO_x catalysts as discussed above and shown in Table 2. The

white-line intensity, a signature of the oxidation state of Pt species, increased steadily with a decrease of the Pt loading. This trend suggests that with decreasing Pt loading the Pt atoms became more oxidized. With the same Pt loading of 0.08 wt %, the 250 °C reduction treatment resulted in lower white-line intensity than that of the same catalyst with a 200 °C reduction treatment. The variations in the white line intensity with the Pt loading are consistent with those of the Pt–O coordination number from the EXAFS data (Table 2). Figure 5b shows an aberration-corrected HAADF-STEM image of the 0.08 wt % Pt₁/FeO_x-R200 catalyst clearly revealing the presence of only isolated Pt single atoms dispersed onto the FeO_x nanocrystallites. There were no Pt clusters or NPs in this catalyst. By analyzing the EXAFS, XANES, and HAADF-STEM data, the authors concluded that the 0.08 wt % Pt₁/FeO_x-R200 catalyst contains only isolated Pt single atoms and that these Pt atoms are highly oxidized.⁶⁵

The low loading level of single metal atoms in SACs, however, pushes the limits of the detectability of the X-ray absorption techniques. New detectors and data analysis protocols may need to be developed in order to acquire reasonable signals of dilute single metal atoms present in SACs.¹⁴¹

IR Spectroscopy and Related Techniques. IR spectroscopy has always played a critical role in characterizing supported metal catalysts because it allows direct monitoring of the interaction between the adsorbed (probe) molecules and the surfaces of the solid metal or support.^{142,143} The IR method utilizes the interaction of molecular probes with the solid surface to extract information about the nature of the entity that adsorbs the probing molecule. By monitoring the changes in vibrational frequency and intensity of the probe modes one can, with proper calibration, deduce the properties of the active centers. Time- and temperature-resolved Fourier transform IR (FTIR) spectroscopy may be used to detect intermediate species during a catalytic reaction. As early as late 1970s, Yates et al. detected the presence of single Rh atomic species in their highly dispersed Rh catalysts via IR spectroscopy technique.¹⁴⁴ The FTIR technique was used to identify the presence of

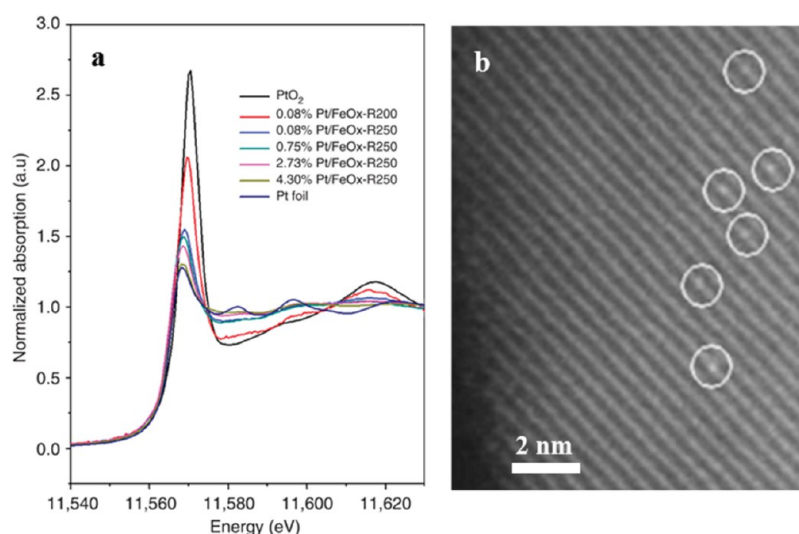


Figure 5. Normalized XANES spectra at Pt L_{III}-edge of different Pt/FeO_x samples (a). The increased white-line intensity with decreasing Pt loading indicates that Pt single atoms are more positively charged (oxidized) than their nanocluster and nanoparticle counterparts. Aberration-corrected HAADF-STEM image of the 0.08 wt % Pt₁/FeO_x-R200 catalyst (b) clearly reveals the isolated Pt single atoms (bright dots within the white circles) dispersed on the FeO_x surface. Adapted from ref 65.

isolated Pt single atoms in H-Mordenite supported Pt catalysts.¹⁴⁵ Recently, diffuse reflectance infrared Fourier transform spectroscopy (DRIFTS) with known site-specific extinction coefficients was used to quantify the fraction of isolated single atom Rh sites in supported Rh catalysts that consist of mixtures of Rh single atoms and NPs.^{134,135} The time- and temperature-dependent IR spectroscopy was used to elucidate the roles of zeolites and metal oxides supported Pt single atoms and NPs for CO oxidation and water–gas-shift reactions.¹⁴⁶ Figure 6 shows an example of how to utilize the

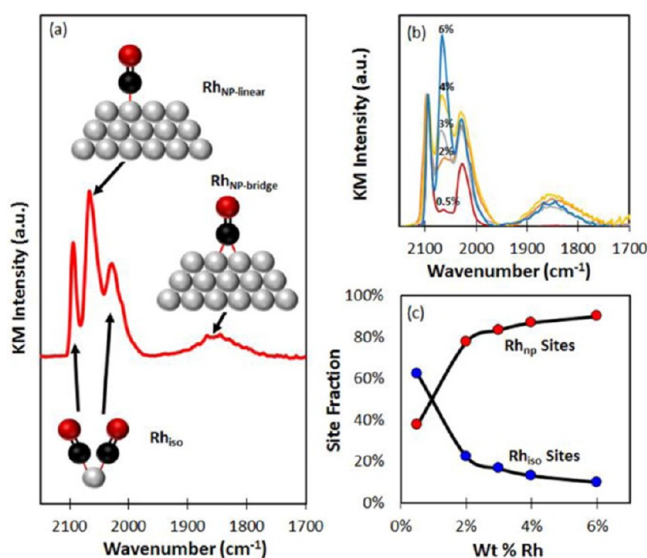


Figure 6. (a) DRIFT spectrum obtained from a saturated layer of CO adsorbed at 300 K on 4 wt % Rh/TiO₂. Insets show ball-and-stick models of assigned vibrational modes. (b) DRIFT spectra of CO on five weight loadings (wt %) of Rh/TiO₂ catalysts. The spectra are displayed in Kubelka–Munk (KM) units and normalized by the symmetric gem-dicarbonyl peak (2097 cm⁻¹) height to allow for comparison. (c) Site fraction (%) of isolated (Rh_{iso}) and nanoparticle-based Rh sites (Rh_{np}), calculated from the spectra shown in (b), as a function of wt % Rh. Adapted from ref 134.

DRIFT technique to extract information about the nature of metal SACs.¹³⁴ The CO was used as the probe molecule and CO adsorption was performed at 300 K on a fresh, reduced 4% Rh/TiO₂ catalyst (Figure 6a). The authors assigned the peaks at ~2097 and ~2028 cm⁻¹ to symmetric and asymmetric stretches of the Rh(CO)₂ gem-dicarbonyl species that exist uniquely at Rh_{iso} sites on the TiO₂ support. The peaks at 2068 and 1860 cm⁻¹ are associated with CO molecules adsorbed in linear and bridge bound geometries at the surfaces of Rh NPs. The DRIFT spectra from different Rh loadings clearly show the peak intensity variations in the linear CO adsorption on the isolated Rh single atom sites (Figure 6b). The fractions of each site type (Rh_{iso} and Rh_{np}) can be quantified and are shown in Figure 6c. These data show that at the lowest Rh weight loading (0.5 wt %), a large number of Rh single atoms exists on the TiO₂ support (~62%). When the Rh loading was increased to 2 wt %, the relative percentage of Rh single atoms dropped significantly to <20%. These data suggest that with very low levels of Rh loading, the Rh mostly existed as isolated single atoms. With increasing levels of Rh loading, Rh clusters or NPs were formed.

The advantages of the DRIFT technique include quantification and in situ monitoring during a catalytic reaction. The

combination of this technique with HAADF-STEM and EXAFS/XANES provides a powerful tool box for studying metal SACs. With extremely low levels of metal loading or mixtures of both single metal atoms and NPs the sensitivity and detection limit of the IR related techniques need to be further investigated.

Nuclear Magnetic Resonance (NMR) Spectroscopy Technique. Solid state magic-angle spinning NMR, especially performed under *in situ* conditions, can provide information about the nature of metal species and binding ligands during a catalytic reaction.¹⁴⁷ This technique has been effectively utilized to study the anchoring of Pt, at low loading levels, on alumina supports.¹⁴⁸ Coordinatively unsaturated penta-coordinated Al³⁺ centers on γ -Al₂O₃ support surfaces were identified to serve as the anchoring sites for Pt single atoms.¹⁴⁸ A recent report on strong NMR signal enhancement, due to parahydrogen-induced polarization (PHIP), was used to detect the presence of Au single atoms.¹⁴⁹

5. CATALYSIS BY SINGLE-ATOM CATALYSTS

There are many examples reported in the past few years that have unambiguously demonstrated the catalytic behavior of supported metal atoms: Metal single atoms mediate catalytic reactions. In many cases, SACs not only are catalytically active but also provide the highest activities and can be extremely stable during catalytic reactions, primarily due to the strong bonding between the single metal atoms and the corresponding anchoring sites on the support surfaces. The fact that isolated single metal atoms dispersed on the appropriate support surfaces can yield excellent catalytic performance opens the door to another frontier of heterogeneous catalysis. We discuss below a few selected examples to demonstrate the capability and great potential of catalysis by supported single metal atoms.

5.1. Oxidation Reactions. SACs have demonstrated great potential in a variety of oxidation reactions, including CO oxidation or preferential oxidation (PROX) of CO in hydrogen-rich stream,^{40,76,82} aerobic oxidation of alcohols,¹⁵⁰ formaldehyde oxidation,^{59,151} methane oxidation,¹⁵² and oxidation of benzene at room temperature,¹⁵³ etc. For both CO oxidation and PROX, experimental results indicate that the Pt₁/FeO_x SAC is 2–3 times more active than the subnanometer-sized counterparts and is stable during a long-term test.⁴⁰ An activity dependence on metal particle size was studied on Pd/meso-Al₂O₃ catalysts and the conclusion is that SACs were most active in the alcohol oxidation reaction.¹⁵⁰ Metiu and co-workers reported that the catalysts containing more isolated ionic Pt atoms are more active for methane oxidation.¹⁵² We only discuss below a few selected examples to illustrate the recent broad applications of metal SACs for oxidation reactions.

CO Oxidation on Au₁/FeO_x SACs. Excellent activity and stability for CO oxidation on a FeO_x supported Au₁ SAC (Au₁/FeO_x) with an Au loading level of only 0.03 wt % (300 ppm) has been achieved.⁷⁶ On the basis of detailed analyses of the experimental data, the authors unambiguously concluded that single Au atoms supported on FeO_x are as active as the Au NPs in the size range of 2–3 nm. A TOF of ~0.5 s⁻¹ was obtained, comparable to those of the best supported Au NPs for CO oxidation. The experimental data unambiguously demonstrated the high activity of supported single Au atoms for CO oxidation. Figure 7a shows that the Au₁ SAC is much more sintering resistant than the Au NP catalysts and exhibited extremely high reaction stability for CO oxidation in a wide

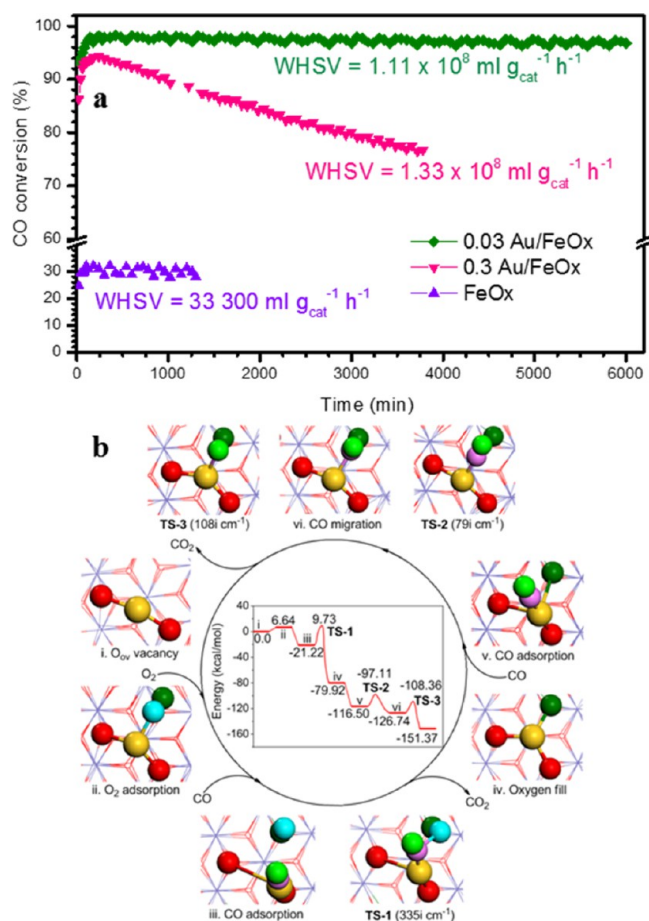


Figure 7. Stability tests of 0.03 wt %Au₁/FeO_x and 0.3 wt %Au/FeO_x catalysts for CO oxidation at 200 °C (a). The test for the FeO_x support is shown as a reference. Test condition: 1 vol % CO + 1 vol % O₂ + 98 vol % He. The weight-hourly space velocity (WHSV) is indicated in the plot. Proposed reaction pathway for CO oxidation on Au₁/FeO_x SAC (b). The inset shows the calculated energy profile with the partially reduced FeO_x as the zero-reference for the energies (in eV). O_{A1} (red) and O_{A2} (red) represent the O atoms on the two sides of a single Au₁ atom (yellow), O_B (light blue), and O_C (dark green) denote the upper and lower O atoms in the adsorbed O₂, and O_D (light green) and C (pink) are the O and C atoms in the CO molecule, respectively. Adapted from ref 76.

temperature range. DFT calculations revealed that the surface-anchored and positively charged Au₁ atoms of high valent states form significant covalent metal–support interaction.⁷⁶ The stability of the Au₁ single atoms originates from such covalent bonding. The degree of covalent bonding becomes weaker for Au clusters and NPs.

The proposed reaction pathways for CO oxidation on the Au₁/FeO_x SACs as well as the calculated energy profile (with the partially reduced FeO_x system as the zero-reference for the energies (in eV)) are shown in Figure 7b. With this proposed mechanism, the presence of the Au₁ atoms facilitates the formation of oxygen vacancies which can dissociatively adsorb O₂ molecules. During the CO oxidation process, a CO molecule adsorbs onto the Au₁ atom and combines with one of the dissociatively adsorbed oxygen atoms to release the first CO₂ molecule. When another CO molecule adsorbs onto the Au₁ atom again it combines with the second oxygen atom (who occupies the original oxygen vacancy site) to release the second CO₂ molecule and thus regenerates the oxygen vacancy to

complete the catalytic cycle. From this perspective, the ability of single metal atoms to facilitate the generation of oxygen vacancies and to appropriately adsorb CO molecules determines the catalytic performances of the supported metal SACs. As we will discuss next, for nonreducible oxide supports, the reaction may proceed along different pathways. The DFT calculations further indicate that the binding of the Au₁ to the oxygen atoms is much stronger than its binding to another Au atom or Au NPs, indicating a strong metal–support interaction (SMSI) between the Au₁ atoms and the FeO_x support surfaces.

CO Oxidation on Pt₁/θ-Al₂O₃ SACs. Metal single atoms dispersed onto nonreducible metal oxides have been investigated for CO oxidation as well. For example, Moses-DeBusk et al. prepared Pt₁/θ-Al₂O₃ catalysts and investigated their catalytic behavior for CO oxidation.¹⁵⁴ By using DFT calculations, the authors found that, in this case, the supported Pt single atom prefers to bond to O₂ instead of CO. After O₂ adsorption on the Pt₁ atom, the CO then bonds to the O₂ to form a carbonate, which can dissociate to release a CO₂. Subsequent reaction with another CO molecule produces the second CO₂ and completes the catalytic cycle. By using in situ DRIFTS study of CO adsorption on the supported Pt single atoms, the authors confirmed the presence CO₃ at room temperature.¹⁵⁴ On the basis of the characterization data and DFT calculations, a pathway for CO oxidation on Pt₁/θ-Al₂O₃ was proposed (Figure 8). The adsorption of O₂ and CO on an

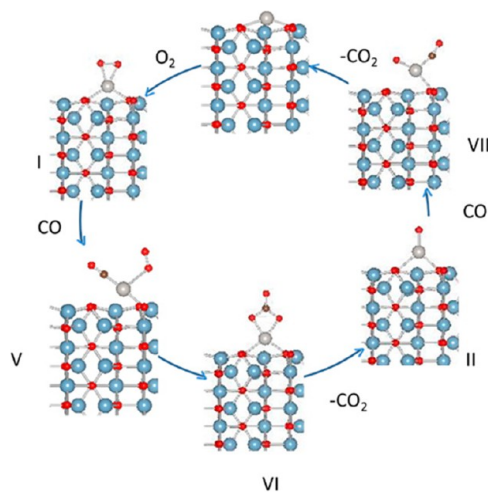


Figure 8. Pathway for CO oxidation on Pt single atoms supported on the (010) surface of θ-Al₂O₃. See text for the discussion of the catalytic cycle. Adapted from ref 154.

oxidized Pt atom creates intermediate V, which is a d¹⁰ Pt species with filled d orbitals. The molecular oxygen, bonded in monodentate mode, is attached to the Pt. The adsorbed CO then interacts with the oxygen to form a carbonate (VI). The carbonate–Pt–O complex is analogous to (Ph₃P)₂Pt(CO₃) which is a Pt(II) complex. Release of CO₂ from the carbonate (VI) leads to II, which then reacts with another CO molecule to form VII. The release of the second CO₂ from VII regenerates the catalytic site and completes the catalytic cycle. Since the inert support cannot provide the required oxygen for the oxidation reaction to proceed, it is claimed that a Pt single atom is catalytically active for CO oxidation without the involvement of the support.¹⁵⁴

The above proposed mechanism of CO oxidation on Pt₁/θ-Al₂O₃ is very different from that on Au₁/FeO_x (Figure 7) or

Pt₁/FeO_x⁴⁰ where the oxygen vacancies on the support surface play an important role. The presence of defects and anchoring sites on the surfaces of nonreducible metal oxide supports and their interactions with the single metal atoms should be further investigated. Further experiments are needed to investigate the effect of the presence of single metal atoms on the local reducibility of the nonreducible metal oxides.

Preferential Oxidation of CO on Au₁/CeO₂ SACs. When Au atoms are dispersed onto CeO₂ nanocrystallites the Au₁/CeO₂ SACs are highly active, selective, and extremely stable for PROX at the PEMFC (proton exchange membrane fuel cell) working temperatures (~80 °C) with >99.5% CO conversion over a wide temperature range of 70–120 °C (or 50–100 °C, depending on the Au loading) (Figure 9).⁸² The high CO

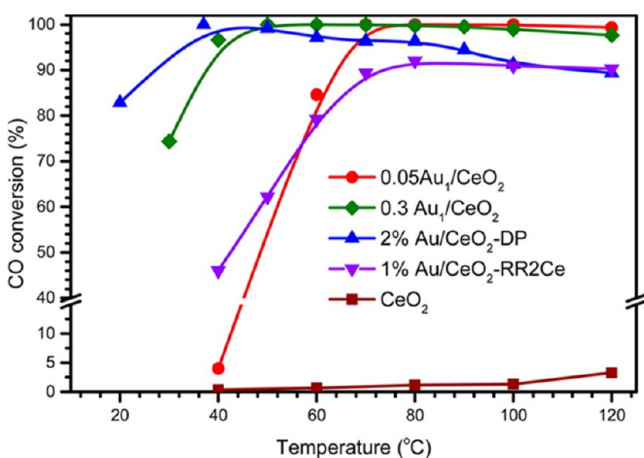


Figure 9. Conversion as a function of reaction temperature for PROX on Au/CeO₂ catalysts. Reaction conditions: 1 vol % CO + 1 vol % O₂ + 40 vol % H₂ balanced with He. Weight-hourly space velocity (WHSV) = 25 000 mL g_{cat}⁻¹ h⁻¹. The Au₁/CeO₂ SACs outperform their nanoparticle counterparts at higher reaction temperatures. Adapted from ref 82.

conversion realized at high temperatures is attributed to the unique property of supported Au₁: A single atom of Au is unable, or at least has a much lower reactivity, to dissociatively adsorb H₂ and thus significantly reduces the activity for oxidation of H₂. On the other hand, Au clusters or NPs significantly oxidize H₂ at temperatures >80 °C. Therefore, Au NPs and clusters are not suitable for high-temperature PROX reactions. Such a strategy of shifting the competitive adsorption behavior of different reactant molecules can be used to design catalysts for targeted performances. We have found that Au single atoms dispersed onto various types of oxide supports can be utilized for a variety of catalytic reactions. Even a tiny amount of 30 ppm Au single atoms dispersed on FeO_x can provide appreciable activity for CO oxidation (unpublished results from the author's lab).

Electrocatalytic Oxidation of Methanol on Pt₁/Graphene SACs. By anchoring isolated Pt₁ single atoms to graphene nanosheets via ALD technique, the synthesized Pt₁/graphene SAC was evaluated for electrocatalytic oxidation of methanol. The reported activity is 10 times higher than that of their NP counterparts.⁶² Furthermore, the Pt₁/graphene SAC demonstrated a much higher tolerance to CO poisoning of the anode which is a major challenge to broad applications of direct methanol fuel cells. It is proposed that the low-coordination and partially unoccupied density of states of the 5d orbitals of

the Pt single atoms is responsible for the observed excellent catalytic performance.

Electrocatalytic Oxidation of Formic Acid on Pt₁/Au SACs. The electrocatalytic oxidation of formic acid can proceed via HCOOH → CO₂ + 2H⁺ + 2e⁻ (direct pathway) or HCOOH → H₂O + CO_{ads} (indirect pathway). The generation of CO_{ads} at low potentials, poisons the electrode and thus prohibits the oxidation of formic acid. Ensembles of Pt atoms direct the reaction toward the indirect pathway. Isolated Pt single sites are highly desirable for formic acid oxidation. By systematically investigating the effects of Pt coverage on well-defined {111} surfaces of Au octahedra on formic acid oxidation it is found that Pt single atoms dispersed onto the Au octahedra provide the best activity for the direct pathway (Figure 10).¹⁵⁵ By

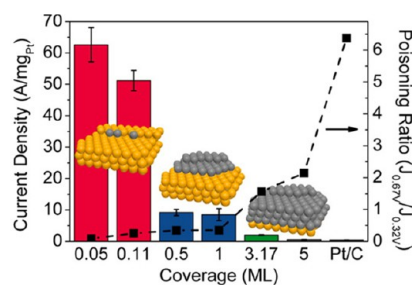


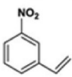
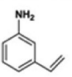
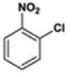
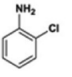
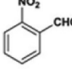
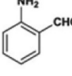
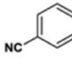
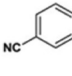
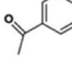
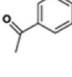
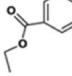
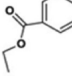
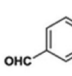
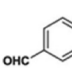
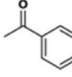
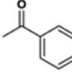
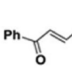
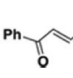
Figure 10. Activity dependence on the Pt coverage of Au {111} surfaces for electrocatalytic oxidation of formic acid. The highest activity and least poison by adsorbed CO species are achieved with Pt monomers or dimers. Adapted from ref 155.

replacing the Au octahedra with a much less expensive TiN substrate to support the Pt₁ single atoms high activity for formic acid oxidation was observed as well.¹⁵⁶ These results exemplify the effective utilization of the unique features of metal SACs to direct catalytic reactions toward desirable products.

5.2. Hydrogenation Reactions. The first hydrogenation reaction carried out on a metal SAC is probably by Xu and co-workers on a series of Au/ZrO₂ catalysts.⁴⁷ They found that a small number of isolated Au³⁺ ions dispersed on a ZrO₂ surface provided high catalytic activity for the selective hydrogenation of 1,3-butadiene. Both the TOF and the specific rates of these isolated Au³⁺ species are orders of magnitude higher than those of the Au NPs. The recent successful synthesis of a variety of metal SACs significantly broadens their applications in hydrogenation/dehydrogenation reactions.

Hydrogenation of Nitroarenes on Pt₁/FeO_x SAC. The catalytic hydrogenation of nitroarenes is an environmentally friendly strategy for the production of anilines which are key intermediates for manufacturing pharmaceuticals, agrochemicals, and dyes. The supported precious metal NPs suffer from low chemoselectivity when one or more reducible groups is present in a nitroarene molecule. The Pt single atoms, when anchored onto FeO_x nanocrystallites, are highly active, chemoselective, and reusable for hydrogenation of a variety of substituted nitroarenes (Table 3).⁶⁵ For hydrogenation of 3-nitrostyrene on Pt₁/FeO_x SAC, it yielded a turnover frequency of 1500 h⁻¹, which is about 20 times as high as the best result reported in the open literature. Furthermore, a selectivity to 3-aminostyrene of about 99%, which is the highest reported value for a Pt group metal catalyst, was reported. The exceptional catalytic performance is attributed to the positively charged (oxidized) Pt single atoms anchored onto the FeO_x surfaces

Table 3. Chemoselective Hydrogenation of Different Substituted Nitroarenes over 0.08 wt %Pt₁/FeO_x-R250 Catalyst^a

Entry	Substrate	Product	Time (min)	Conv. (%)	Sel. (%)
1			50	96.5	98.6
2			60	100	97.4
3 [*]			44	96.9	98.0
4 [*]			120	90.3	97.8
5			30	93.4	99.4
6 [†]			122	93.7	99.3
7 [†]			80	99.5	92.8
8			114	95.9	99.7
9 [‡]			10	100	90

^aReaction conditions: $T = 40\text{ }^{\circ}\text{C}$, $P = 3\text{ bar}$, 0.08 wt % Pt₁/FeO_x catalyst, Pt/substrate = 0.08%; 5 mL of reaction mixture: 0.5 mmol substrate, toluene as solvent, O-xylene as internal standard. ^{*}Pt/substrate = 0.32%, $T = 50\text{ }^{\circ}\text{C}$, $P = 6\text{ bar}$. [†]Pt/substrate = 0.16%. [‡]Pt/substrate = 0.41%, refer to yields of isolated products. Adapted from ref 65.

and the absence of Pt–Pt bonds. This work clearly demonstrates the power of supported metal SACs for catalytic conversion of important molecules.

Selective Hydrogenation of Styrene and Acetylene on Pd₁/Cu SACs. Adsorption and rapid dissociation of reactant molecules, and appropriate binding of intermediates are critical to efficient and selective catalysis. However, to construct an active center that performs all these functions, although technologically important, is a major challenge. By placing isolated Pd atoms on a Cu surface, one can substantially lower the energy barrier to both dissociation of H₂ molecules (on Pd atoms) and the subsequent desorption of the product molecules from the Cu metal surface.⁵² Such a facile hydrogen dissociation on Pd atom sites, spilling over to Cu sites, and weak binding of Cu to the product molecules allow for selective hydrogenation of styrene and acetylene as compared to using pure Cu or Pd metal alone.⁵² The ability of single metal atoms to adsorb and dissociate molecules opens many possibilities for designing complex multifunctional catalysts to achieve desired activity and selectivity.

Selective Hydrogenation of 1,3-Butadiene to 1-Butene on Pt₁/Cu SACs. The design of a series of Cu supported Pt SACs and the application of these to the selective hydrogenation of 1,3-butadiene to 1-butene, an industrially important reaction, are further proof of the unique catalytic applications of manipulating atomic species to achieve desired catalytic reactions (Figure 11).¹⁵⁷ The multistep reaction sequence

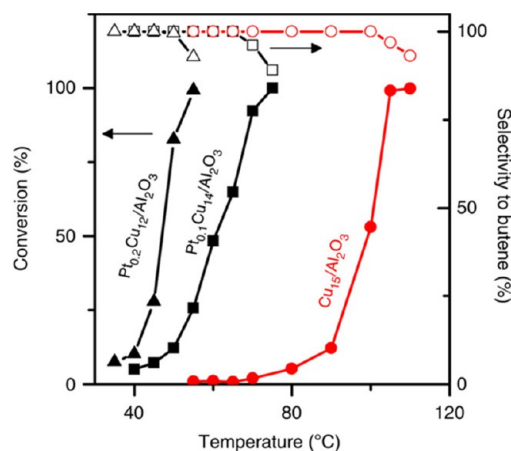


Figure 11. Hydrogenation shown as a function of temperature over Cu₁₅/Al₂O₃, Pt_{0.1}Cu₁₄/Al₂O₃ and Pt_{0.2}Cu₁₂/Al₂O₃ NPs. Reaction conditions: 1,3-butadiene (1.25%), H₂ (20%), and He (balance); GHSV = 1200 h⁻¹. Adapted from ref 157.

clearly demonstrates the potential of designing SACs for desired catalysis: The isolated Pt atom on Cu activates H₂ molecules, which subsequently spillover to the Cu surface, leading to hydrogenation without affecting the C–C bond scission. The authors found that with a ratio of <1 Pt atom per 100 Cu atoms the Pt₁/Cu SAC exhibited high activity and selectivity for butadiene hydrogenation to butenes under mild conditions.¹⁵⁷ Such a design of catalytic centers not only enhances the selectivity of the catalyst but also its long-term stability.

Selective Hydrogenation of 1-Hexyne to 1-Hexene on Pd₁/C₃N₄ SACs. By anchoring individual Pd atoms onto highly porous and inexpensive C₃N₄, an excellent and thermally stable catalyst was synthesized and used to perform catalytic hydrogenations including the conversion of 1-hexyne to 1-hexene, selectively converting the C≡C triple bonds without degrading the C=C double bonds.⁷⁷ This catalyst has demonstrated a superior activity and selectivity to those of the Pd NPs. The C₃N₄-supported Pd SAC was extremely stable during the hydrogenation reaction due to the strong bonding of the Pd atoms to the N atoms of the C₃N₄ support (Figure 12).^{77,158,159}

5.3. Water–Gas-Shift (WGS) and Reforming Reactions. WGS Reaction on Au₁ and Pt₁ SACs. By leaching out the metal NPs from supported metal catalysts, Flytzani-Stephanopoulos and co-workers discovered that the performance of the leached catalysts for WGS reaction did not change.^{46,49,67,79} Further characterization of the leached catalysts revealed the presence of positively charged, isolated metal ions. This research group has experimentally established that both positively charged Pt and Au single atoms supported on appropriate oxides are the active species for WGS reactions. They further proposed that the intrinsic activity of the M₁–O_x(OH)–S site, where M₁ is a metal ion and S is a support, is the same for any support and

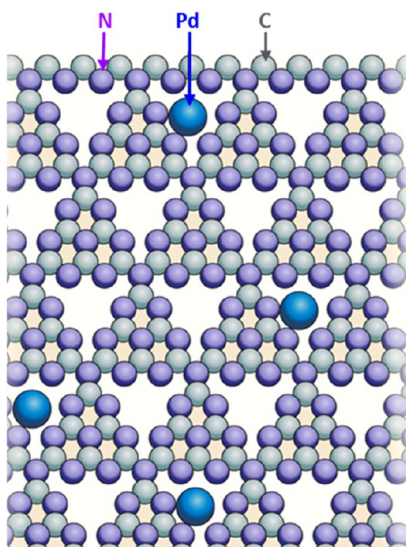


Figure 12. Isolated Pd atoms anchored onto porous C_3N_4 act as catalysts for hydrogenation reactions. Strong bonds to the nitrogen atoms firmly anchor the Pd atoms inside the roughly triangular pores in the stacked, two-dimensional layers of C_3N_4 . Only one layer is depicted, for simplicity. Adapted from ref 158.

that the support effect is indirect, only providing a physical surface to carry the metal species. By adding alkaline species to the $M_1-O_x(OH)-$ complexes, the active centers can be tuned, attached to nonreducible oxides, and stabilized.⁷⁹ For both Au_1 - and Pt_1 -based SACs, regardless of the nature of the support materials and the catalyst preparation methods, all the supported Au_1 and Pt_1 SACs, for WGS reaction, yielded the same apparent activation energy and TOF (Figure 13). The identification of such uniform single sites for specific catalytic reactions is important and provides deep insights into the understanding of the supported metal SACs and their unique properties for specific catalytic reactions. The experimental data generated in our lab suggest that for WGS reactions on SACs, it is highly plausible that H_2O molecules not only act as reactant molecules but also act as promoters for the WGS and other catalytic reactions. In these particular cases, the presence of OH groups on the support surfaces may function as a buffer layer between the single metal atoms and the surface atoms of the support. The interaction of the single metal atoms with the support surface may be significantly modified by the presence of the OH groups.

Methanol Steam Reforming on Pt_1/ZnO and Au_1/ZnO SACs. Single Pt_1 and Au_1 atoms stabilized by lattice oxygen on the $\{10-10\}$ surfaces of ZnO nanowires were used for methanol steam reforming (MSR).⁶⁸ DFT calculations suggest that the strong bonding of the Pt_1 and Au_1 single atoms to the lattice oxygen resulted in stronger binding toward the intermediates, lowering reaction barriers, modulating the reaction pathways, and thus greatly enhancing the activity (Figure 14). The measured TOF of the single Pt_1 sites is about 3 orders of magnitude higher than that of the pristine ZnO , which is active for MSR as well. Not only the activity of the Pt_1/ZnO SAC is much higher than that of the Au_1/ZnO , the CO selectivity of the Pt_1/ZnO is very different from that of the Au_1/ZnO as well, clearly demonstrating the fact that the performance of the metal SACs strongly depends on the right combination of the metal and the support.

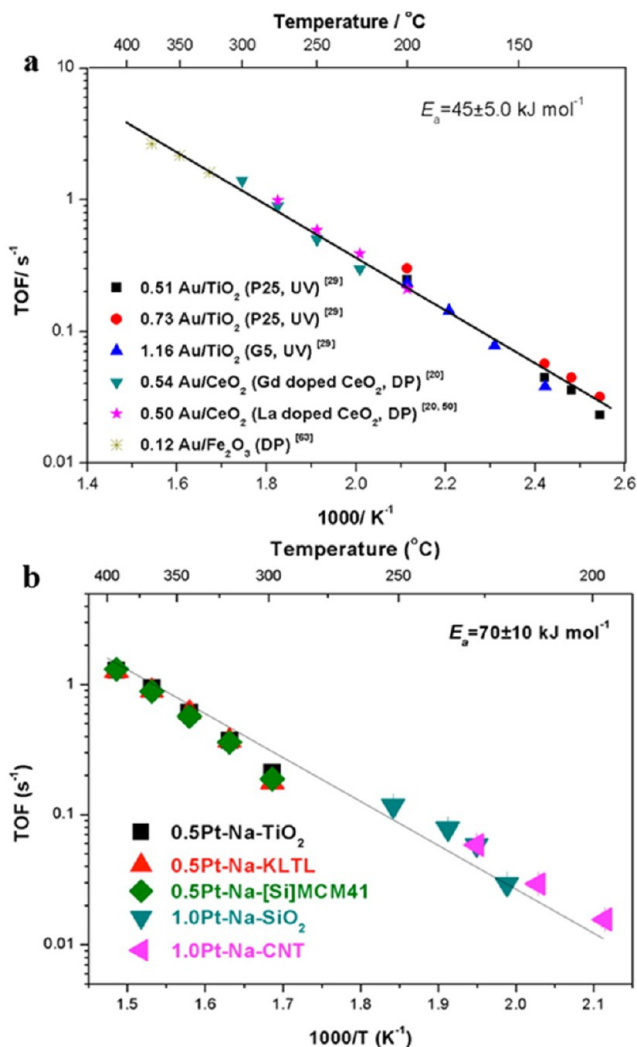


Figure 13. TOF plot for the WGS reaction over leached Au/CeO_2 , Au/Fe_2O_3 , and Au/TiO_2 catalysts (a) and over the Na-containing Pt catalysts on various supports (b) in a simulated reformate gas mixture 11% $CO-26\% H_2O-7\% CO_2-26\% H_2-He$. DP, deposition-precipitation; UV, UV-assisted DP. The numbers are the weight percentages of Au or Pt in each sample. P25, 30% rutile +70% anatase from Degussa; G5, 100% anatase from Millenium. Panel a is adapted from ref 67, and panel b is from ref 79.

5.4. Electrocatalytic Reactions. Electrochemical Synthesis of H_2O_2 on M_1 SACs. The direct electrochemical synthesis of H_2O_2 is strongly desirable. The commercial viability of such a process, however, strongly depends on the effective catalysts to reduce oxygen at the cathode. Isolated Pt single atoms are crucial for achieving high selectivity to hydrogen peroxide because the availability of two Pt adjacent active sites can dissociatively adsorb O_2 , which is highly undesirable.¹⁵⁹ Metal SACs are particularly fitted to this type of catalysis because they possess only isolated single atom sites.

By preparing highly porous zeolite-templated carbon (ZTC) with large amounts of S-functionalities and highly curved three-dimensional networks of graphene nanoribbons, high loading levels of Pt single atoms have been achieved.¹⁶⁰ The ZTC contains bucky-bowl-like nanographenes linked into three-dimensional networks, providing a large number of graphene edge sites ready to incorporate the S-functional groups.¹⁶⁰ The Pt single atoms strongly bind to the thiophene- and thiolate-like

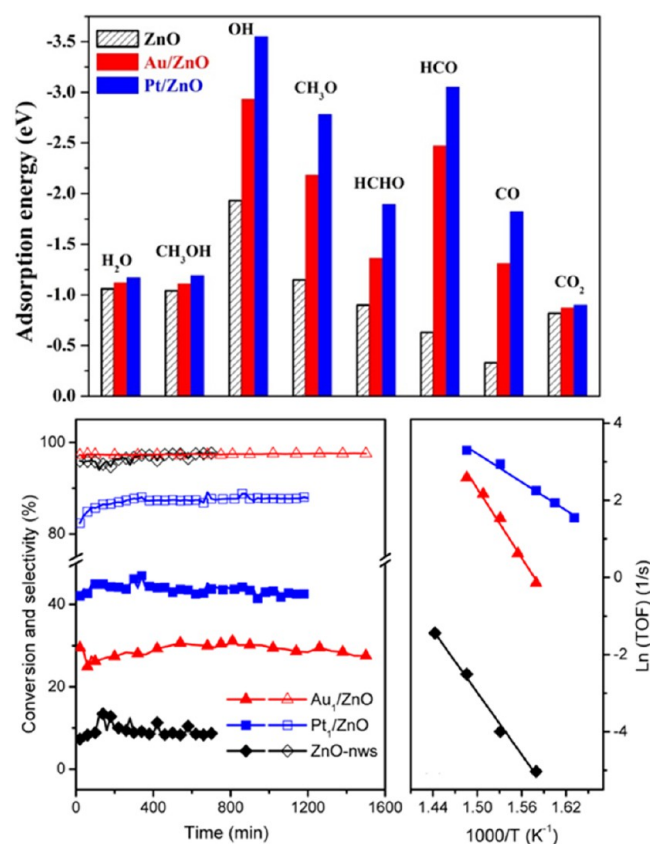


Figure 14. Top panel: Calculated binding energies of the reactants and intermediates involved in MSR on ZnO{10–10} (shadow), Au₁ (red solid) and Pt₁ (blue solid) embedded ZnO{10–10}. Bottom panel: Methanol conversion (solid) and CO₂ selectivity (open) as a function of reaction time at 390 °C on Au₁/ZnO (red triangle), Pt₁/ZnO (blue square) SACs and the pristine ZnO nanowires (black diamond); and the corresponding Arrhenius plots of the reaction rate Ln (TOF) (s⁻¹) versus 1/T for the MSR reaction. Adapted from ref 68.

functional groups at the graphene edge sites to form Pt–S₄ complexes. During the O₂ reduction process, the synthesized catalyst does not follow the conventional four-electron pathway to generate H₂O but selectively produces H₂O₂ via the two-electron pathway.¹⁶⁰ On the basis of the experimental results and DFT calculations, the authors proposed a catalytic cycle involving the two-electron pathway electrochemical synthesis of H₂O₂ on Pt₁–S₄ complexes (Figure 15). Such Pt₁/C SACs may have potential for effective electrocatalytic production of important chemicals such as H₂O₂.

By placing Pd atoms onto Au NPs, electrocatalytic production of H₂O₂ directly from H₂ and O₂ has been realized.⁵¹ It is proposed that the enhancement toward H₂O₂ selectivity is due to the presence of individual surface Pd₁ atoms surrounded by Au atoms; surface ensembles of contiguous Pd atoms would direct the selectivity to formation of H₂O. This is another example of manipulating the nature of the catalytically active single metal atom centers for better selectivity.

Electrocatalytic Water Splitting on Co₁/N-Doped Graphene SAC. Electrochemical reduction of water to produce hydrogen is a clean and sustainable approach to generating H₂. Platinum has been considered to be the best catalyst for the hydrogen evolution reaction (HER) at the cathode, but its high cost prohibits the wide applications of such a catalyst. Cobalt single atoms anchored onto N-doped graphene have proven to

be an effective and durable catalyst for the electrocatalytic water splitting reaction (Figure 16).⁷⁸ The electrocatalytic performance of the Co₁/N-doped graphene SACs proved to be excellent with an intrinsic activity per Co atom similar to, or higher than, that of most non-noble metal catalysts and the SAC is durable in both acidic and basic media. The SACs can simply be fabricated by heating graphene oxide with a small amount of cobalt salt in a nitrogen-containing gas environment. The presence of Co or CoO_x clusters is detrimental for the HER. Only Co single atoms strongly bonded to the N of the N-doped graphene provide the best HER performance. The Co–N interaction is critical to creating the Co–N active sites. Since the synthesis processes are simple and scalable such low-cost, non-noble-metal-based SACs provide a promising candidate to replace Pt NPs for water splitting applications.

Oxygen Reduction Reaction on M₁ SACs. Nitrogen-doped porous carbon materials containing metals (e.g., Co, Fe, Nb, etc.) have been used for the oxygen reduction reaction (ORR). The recent experimental data clearly demonstrated that when the single metal atoms are strongly coordinated to C, N, or other functional groups they provide excellent performances for the ORR.^{161–163} For these types of metal SACs, the catalytically active centers seem to be well-defined: The metal M₁ is coordinated to nitrogen atoms to form coplanar M₁–N_x–C complexes. The high ORR activity of the M₁–N_x–C active sites is likely attributable to the moderate adsorption strength of key ORR intermediates on these active sites.

5.5. Other Types of Catalytic Reactions. Since metal SACs are a subset of supported metal catalysts, they should be evaluated for all types of catalytic reactions. We list below a few recent examples and it is expected that a wide variety of catalytic reactions will be tested on various types of SACs in the near future.

Photocatalysis. Photocatalytic water splitting to produce H₂ is of importance for directly converting solar energy into solar fuels. By embedding Pt single atoms into two-dimensional porous g-C₃N₄ as cocatalyst a remarkable performance for photocatalytic H₂ evolution has been realized.⁸⁹ The embedded Pt single atoms modulate the system's electronic structure (surface trap states), resulting in a longer lifetime of photon generated electrons. The Pt single atom cocatalyst leads to tremendously enhanced photocatalytic H₂ generation, more than 8 times higher than that of Pt NPs.⁸⁹

Aerobic Oxidative Cross-Coupling of Primary and Secondary Alcohols. Formation of C–C bonds is an important class of chemistry for constructing complex large molecules from readily available simple substrates. The current processes often involve the use of organic halides and thus pose environmental issues. Aerobic oxidative cross-coupling of primary and secondary alcohols to directly produce α,β-unsaturated ketones may be realized if appropriate catalysts are developed. By pyrolysis of cobalt–phenanthroline complexes on a mesoporous carbon support, the Co atoms incorporate with the nitrogen and carbon to form Co–N–C complexes which are effective for aerobic oxidative cross-coupling of primary and secondary alcohols.¹⁶⁴ This Co₁/N-doped carbon SAC demonstrated high catalytic activity (TOF of 3.8 s⁻¹ based on Co single atoms, surpassing the state-of-the-art TOF reported in literature), good recyclability, and wide applicability to diverse substrates (28 examples). The active sites of the catalyst are proposed to be Co single atoms bonded with N within graphitic sheets (Figure 17).

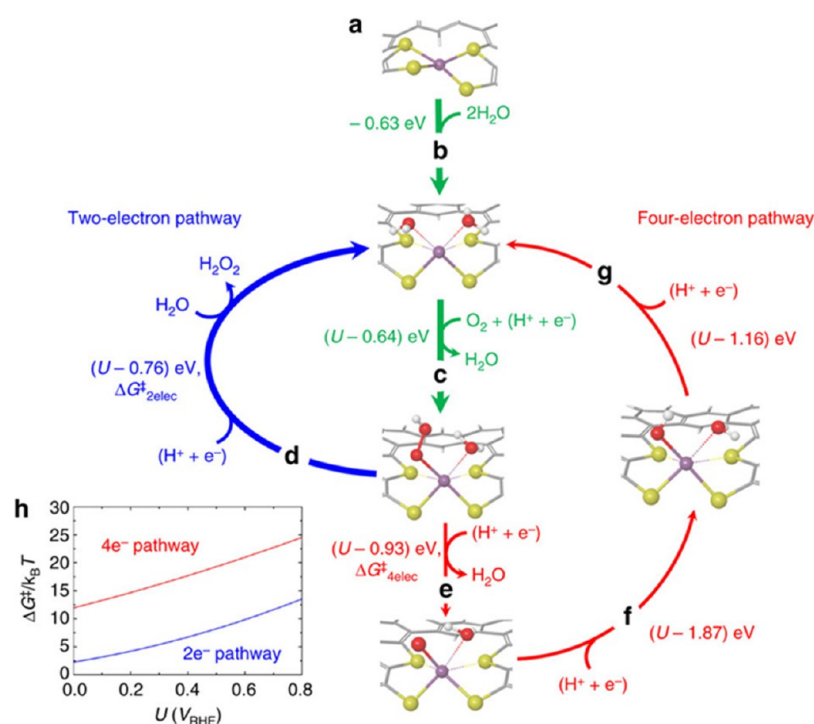


Figure 15. (a) Atomically dispersed Pt (purple) complexed with four sulfur-containing moieties consisting of two thiophene and two thiolate groups that are covalently bonded to a carbon framework. (b) Activation of Pt center by substituting two S (sulfur) of thiophene-like moieties with two O (oxygen) of water molecules. (c) The first reduction of an O_2 via proton-coupled electron transfer (PCET), forming OOH. This is a shared elementary step of the two- and four-electron pathways. (d) Two-electron pathway: H_2O_2 formation by the second PCET and the subsequent substitution of an H_2O_2 molecule with an outer-sphere H_2O molecule, recovering the initial state where Pt is complexed with two thiolates and two water molecules. (e) Four-electron pathway: H_2O formation by the second PCET involving O–O bond dissociation. (f) Four-electron pathway: OH formation by the third PCET to the O atom. (g) The fourth PCET to the OH forms an inner-sphere H_2O , recovering the initial state where Pt is complexed with two thiolates and two waters. (h) Calculated kinetic barriers of the second PCET steps for the two-electron pathway (blue) and the four-electron pathway (red) using Marcus kinetic theory. C: gray, H: white, S: yellow, O: red, and Pt: purple. Adapted from ref 160.

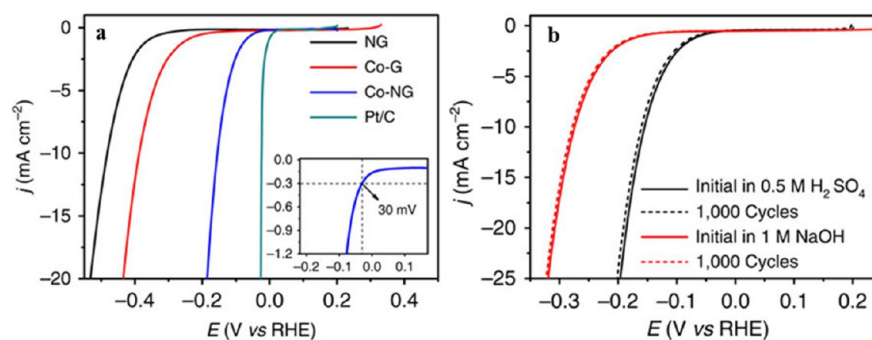


Figure 16. (a) Linear-sweep voltammograms (LSV) of N-doped graphene (NG), Co/graphene (Co-G), Co_1/N -doped graphene (Co-NG), and Pt/C in $0.5 \text{ M H}_2\text{SO}_4$ at a scan rate of 2 mV s^{-1} . The inset shows the enlarged view of the LSV for the Co-NG near the onset region. (b) Accelerated stability measurements by recording the polarization curves for the Co-NG catalyst before and after 1000 cyclic voltammograms at a scan rate of 50 mV s^{-1} under acidic (black curves) and basic conditions (red curves). Adapted from ref 78.

Formic Acid Decomposition on $M_1/\text{Carbon SACs}$. Formic acid, derivable from biomass, possesses a high hydrogen-storage capacity and can be considered as a source of hydrogen for various applications. Formic acid decomposition on supported Pt-group metal NPs have been extensively studied. A recent report, however, found that the decomposition of formic acid proceeds much faster on Pt-group single atoms than on their NP counterparts.¹⁶⁵ The synthesis process is simple and can be easily accomplished by simply anchoring Pt-group metal atoms onto mesoporous N-functionalized carbon nanofibers.¹⁶⁵

Electrodes for Solar Cells. FeO_x supported Pt single atoms were used as counter electrodes (CEs) in dye-sensitized solar

cells (DSCs).⁷⁰ Compared to conventional Pt NP based CEs, the SAC-based CEs exhibited better activity and reversibility.

The broad applications of supported single metal atoms to other types of catalytic reactions, to sensing of molecules, and to energy conversions should be explored in the near future.

6. CATALYTICALLY ACTIVE CENTERS

In his seminal paper “*A Theory of the Catalytic Surface*”, Sir Taylor suggested that unsaturated metal atom sites can control the surface chemical reactivity.¹⁶⁶ Figure 18 displays a modified version of Taylor’s original model of a rough and jagged Ni surface. The different colors represent atoms with different

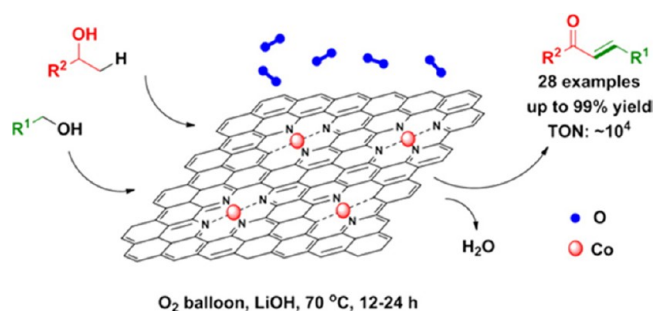


Figure 17. Schematic diagram illustrates the active sites of a Co_1/N -doped graphene SAC for aerobic oxidative cross-coupling of primary and secondary alcohols to directly produce α,β -unsaturated ketones, important intermediates for agrochemical, pharmaceutical, and other fine chemicals. Adapted from ref 164.

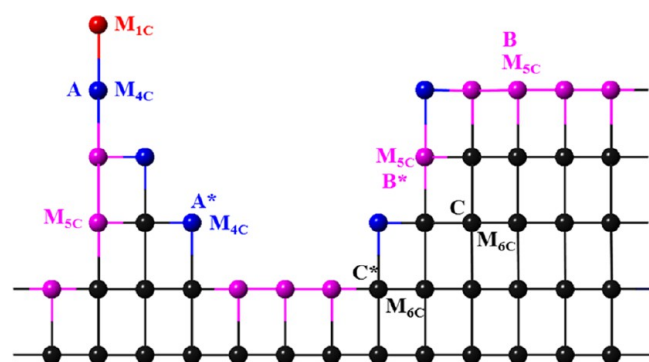


Figure 18. Schematic diagram illustrates the various unsaturated atom sites of a face-centered metal. $M_{\text{NC}}-M$ is metal, and NC is the N coordination number of that metal atom. Color code: red represents coordination 1; blue represents coordination 4; purple represents coordination 5; and black represents full coordination of 6. A and A^* atoms have the same coordination number, but they have different bond lengths with the neighbor atoms. The same is true for B and B^* . C and C^* have the same coordination number and bond lengths with the neighbor atoms, but they have different accessibility by a reactant molecule and different second-nearest neighbors.

coordination numbers. It is interesting to note that even if the metal atoms have the same coordination number they may have different bond lengths with the neighbor atoms or the second nearest neighbors. Due to the presence of “inward corners” (indicated by the letter C^* in Figure 18) on kinked surfaces even fully coordinated corner atoms can be partially accessible

by reactant molecules. Although in theory one can make such rough and jagged metal surfaces and create atom sites with different reactivity, such a surface, in practice, will not be stable. On a metal NP there are a number of other configurations of metal atoms such as steps, kinks, edges, and corners. A critical question is which one of these local geometries are the active sites for a specified catalytic reaction. Since the unsaturated bonds of the different types of surface atoms are very different, they may all do catalysis, but some of the catalytic reactions could be undesirable.

The idea that high-energy surface sites act as active centers for catalytic reactions are not necessarily straightforward or even correct. The Sabatier principle states that the best catalysts should bind atoms and molecules with an intermediate strength: not too weak so they can activate the reactants and not too strong so the products can desorb.¹⁶⁷ Therefore, for every single catalytic reaction, there exists an optimum binding strength. However, how to implement the Sabatier principle to design the appropriate catalyst for a target chemical transformation is extremely challenging. Both Taylor’s active center approach and Sabatier’s general concept of optimum binding strength suggest that one needs to perturb the thermodynamically stable or metastable surface in order to modify its electronic structure with the goal of tuning the binding strength of the relevant molecules. Such an approach has been practiced in the semiconductor industry with tremendous success: Doping a pure semiconductor to modify its electronic band structure and conductivity. We can use the same principle for catalysis applications by engineering the surface electronic structure to tune its binding energy for reactant and/or product molecules. Figure 19 schematically illustrates the concept of “doping” the surface of a metal, metal oxide, or any other types of crystalline supports in order to tune the local electronic structure for optimum binding of reactant molecules.

With the use of metal oxides as supports for SACs, the geometric location of the metal atoms determines how these metal atoms interact with the support surfaces. During the synthesis processes, the metal atoms should be anchored at the sites that maximize their interactions with the support surface in order to minimize the total energy of the system. With low levels of metal loading, experimental examinations of many different types of metal-oxide-based SACs suggest that the sparsely populated and isolated single metal atoms usually occupy exactly the cation positions of the corresponding metal oxides. Figure 20 shows aberration-corrected HAADF-STEM images of (a) Au_1/ZnO , (b) Pt_1/FeO_x , and (c) Pt_1/NiO SACs.

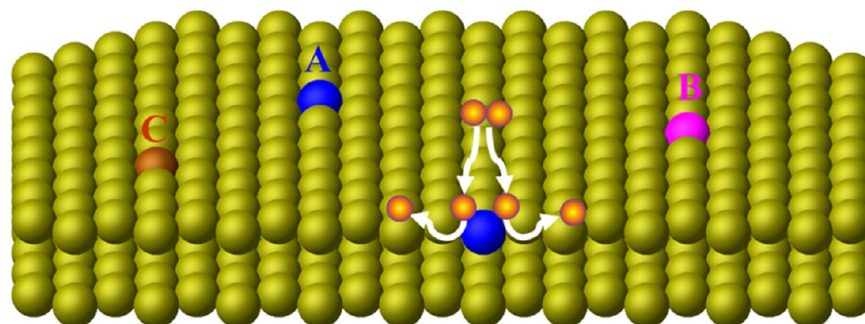


Figure 19. Schematic illustration of incorporating dopant atoms into the surface of a crystalline metal or metal oxide support. The different colors represent different types of dopant atoms (A , B , and C). The small spheres represent dimer molecules (H_2 , O_2 , N_2 , etc.) dissociating on the dopant atom. Depending on the types of the dopants, the local surface electronic structure of the support can be modified, which in turn tunes the binding strength of the reactant molecules.

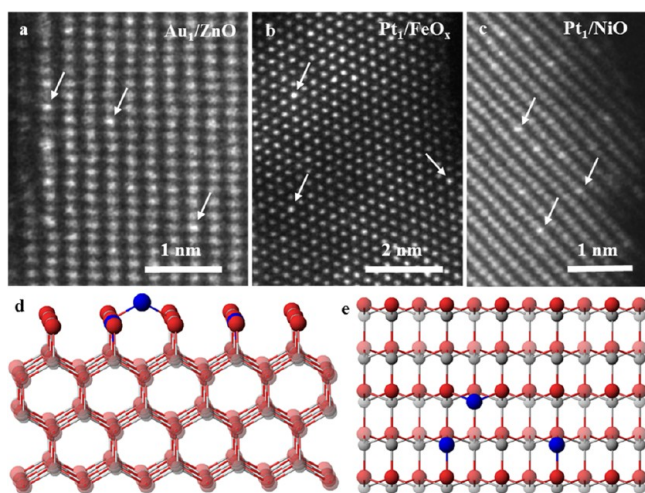


Figure 20. Aberration-corrected HAADF-STEM images of single metal atoms dispersed onto metal oxide supports: (a) Au single atoms on ZnO nanowires, (b) Pt single atoms on FeO_x nanocrystallites, and (c) Pt atoms on NiO nanocrystals. All the images unambiguously show that the single metal atoms occupy exactly the metal cation positions of the metal oxide support. Schematic illustrations of the locations of metal atoms (blue) with respect to the oxygen atoms (red) and Zn atoms (gray) on ZnO {10–10} surfaces: perspective view (d) and plan view (e).

These images unambiguously show that the noble single metal atoms occupy exactly the cation positions of the corresponding metal oxide supports. From these images and many other similar images, one can conclude that either the single metal atoms substitutionally doped the metal oxide surfaces or they were anchored at the positions that the cations of the metal oxide support would occupy; the noble metal atoms seem to prefer to take positions that are extensions of the metal oxide surface. An illustration of the most preferred positions of single metal atoms are shown in Figure 20d (perspective view) and Figure 20e (plan view).

DFT calculations confirm that the most probable sites for Pt single atoms in the Pt_1/FeO_x SACs are the 3-fold hollow sites on the O_3 -terminated surface of FeO_x , where each Pt atom is coordinated by three surface oxygen atoms. The location of the Pt_1 atoms can be viewed as the surface Fe atoms being replaced by Pt atoms.⁴⁰ The noble metal atoms are usually positively charged. Studies of the model catalyst of Au adatoms on the (111) surface of single-crystal magnetite has confirmed that Au single atoms are attached atop an uncapped O atom in the position that would be occupied by tetrahedral Fe ions in a bulk iron oxide crystal.¹⁶⁸ Another STM + DFT study revealed that on Fe_3O_4 (100) the Au adatom is 2-fold coordinated to the surface oxygen atoms which do not have a subsurface Fe_{tet} neighbor.⁵⁷ Furthermore, the DFT + U calculations suggest that the positively charged Au adatoms protrude ~ 0.05 nm above the Fe_3O_4 (100) surface. Interestingly, the Au adatoms resist sintering at temperatures up to ~ 527 °C, reflecting a strong bonding between the Au single atoms and the Fe_3O_4 support surface.⁵⁷

For single metal atoms supported on $\gamma\text{-Al}_2\text{O}_3$, the metal species anchor to the unique defects of the support with metal–O–Al bonding contributions.^{148,150,169} The tunnels of hollandite-type manganese oxide support consist of oxygen with lone-pair dangling electrons. Ag single atom chains can be formed in these tunnels and thus unique single atom sites are

formed.⁵⁹ For SACs with metals as support, the location of single atoms depends on the chemical potential of the constituent metals. For example, because of the higher chemical potential of Au than Pd, the Au atoms prefer to stay on the corner sites of Pd clusters.⁵⁶ For the Pt_1/Cu SAC the Pt single atoms were embedded in the Cu surface, taking the substitutional dopant positions.¹⁵⁷ For SACs with graphene as support, the carbon vacancies or edge sites serve as anchoring sites for metal atoms.^{62,170,171}

From these examples discussed above, one can conclude that the catalytically active centers in the supported metal SACs are the isolated single metal atoms that either anchor at the cation vacancies (or equivalent cation positions) on the metal oxide surfaces (substitutional doping) or at other types of surface defects of the supports.

Metiu and co-workers have extensively investigated, primarily by calculations, the properties of metal doped oxides.^{172–178}

The role of a dopant is to disrupt the chemical bonds in the surface of the oxide so that the oxygen atoms near the dopant can be modified for chemical reactions. Based on their calculations, they extracted some common properties by doped oxides and provided a classification of the dopant–oxide pairs.¹⁷⁸ By using the DFT method to study the chemistry of substitutionally doped oxides with cation dopants having lower valence than that of the host, they proposed two rules: (1) the presence of the dopant makes the oxide a better oxidant and (2) adsorbing an electron donor on the surface counteracts strongly the effect of the dopant. Therefore, depending on the valence of the metal dopant, one has to consider the contribution of the chemical compensation effect on the catalytic behavior of supported metal SACs.

Doping may also activate nonreducible oxides to participate in catalytic reactions that would not occur with the nondoped oxides. Freund and co-workers recently studied the charge transfer between the dopants and the oxygen species, explored the nature of doped oxides, and correlated charge-transfer processes with the distinct adsorption behavior of doped oxides.¹⁷⁹ They discussed the effects of dopants on the electronic structure of the host oxides and the introduction of new states within the large band gaps of nonreducible metal oxides. The presence of subsurface dopants and vacancies may also affect the anchoring and the electronic structure of surface adatoms as well as the adsorbing molecules on these adatoms.

Figure 21 is a schematic diagram illustrating the charge balance in a divalent metal oxide (e.g., NiO, MgO, etc.) due to the presence of cation and anion vacancies, monovalence and trivalence cation doping, and trivalence anion doping. In practice, the charge rebalance due to the incorporation of substitutional cation or anion dopants and the interaction of vacancies with dopants are more complicated. Localized charge transfer may occur on highly insulating supports, but the charge transfer may not be localized on reducible metal oxides. To create more cation vacancies requires doping by high valence metals. A better understanding of surface defects, surface charge transfer, and surface charge redistribution is urgently needed to understand the catalytic behavior of supported metal SACs. DFT calculations may provide guidance on this perspective.

The above discussions are valid for low levels of metal loading. When the number of single metal atoms are much higher than the number of anchoring sites that the support can provide small clusters appear due to the fact that some of the single metal atoms may not be anchored by the defect sites of the support. Figure 22 shows such an example. When higher

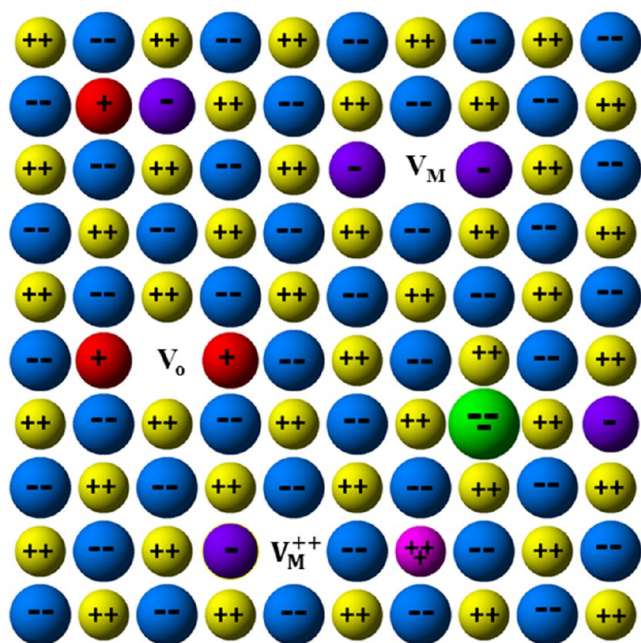


Figure 21. Schematic diagram illustrates the charge balance in a divalent metal oxide (e.g., NiO and MgO) due to the presence of a neutral cation vacancy (V_M), neutral oxygen vacancy (V_O), a positively charged cation vacancy (V_M^{++}), monovalent cation (red color), trivalent cation dopant (pink color), and a trivalent anion dopant (green color). The purple color represents O^- and the red color represents M^+ . The yellow and blue colors represent cations and anions in the metal oxide, respectively.

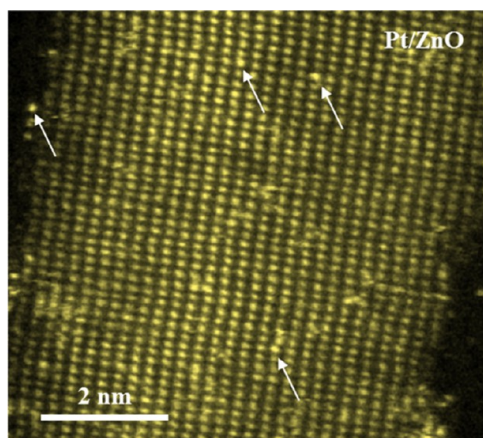


Figure 22. Aberration-corrected HAADF-STEM image of a Pt/ZnO nanowire catalyst shows that some of the Pt atoms, and most of the small Pt clusters were not stable under electron beam irradiation. A few Pt atoms were, however, stable (indicated by the arrows). It is postulated that Pt atoms located at the Zn cation vacancy sites are probably stable under electron beam irradiation (200 kV).

levels of Pt were loaded onto the ZnO nanowires, small Pt clusters were formed. Under electron beam irradiation (200 keV electron beam), almost all the Pt clusters and most of the Pt single atoms were not stable. Careful observations of time-lapsed images reveal, however, that a few Pt single atoms, which were probably anchored by the cation vacancies, were stable, implying various degrees of anchoring of the Pt single atoms.

The number of surface cation vacancies is an important parameter for developing stable metal SACs supported on metal oxides. For example, nanocrystals of ceria, fabricated by

wet chemistry method, possess large numbers of cation vacancies. Some of these vacancies (probably vacancy clusters) are even visible in atomic resolution HAADF-STEM images (Figure 23). Because of the large number of Ce vacancies, high

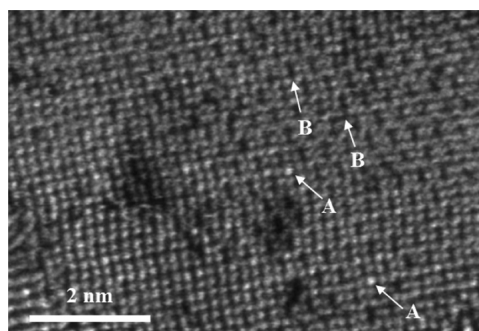


Figure 23. Aberration-corrected HAADF-STEM image of a Au_1/CeO_2 SAC catalyst shows the bright Au atoms (indicated by A) and many clusters of Ce vacancies (indicated by B). The oxygen atoms are not visible under this imaging mode.

levels of Pt or Au single atoms can be accommodated on the surfaces of nanocrystalline ceria. Some of these vacancies most probably reside within the ceria nanocrystallites and these interior cation vacancy sites may accommodate noble single metal atoms as well.

In a series of papers, Flytzani-Stephanopoulos and co-workers proposed that the support surface does not play an important role in determining the catalytic performance of atomically dispersed metal catalysts.^{66,67} They proposed that the catalytic performance, for WGS and steam reforming reactions, is determined by the $M_1-O_x(OH)-S$ sites (where M_1 and S represents single metal atoms and support, respectively). The sole purpose of the support is to provide enough physical surface area to carry the $M_1-O_x(OH)$ -species. The activation energies are almost the same regardless of the nature of the support. Its validity, however, has not been verified for catalytic reactions that do not involve the participation of water. The effects of the OH groups and the promoting behavior of the H_2O molecules need to be carefully evaluated and understood. Our work shows that the OH groups play a major role in anchoring single metal atoms. However, without a continuous supply of H_2O the anchoring effect of the OH groups may not last long at high reaction temperatures.

Analogous to bimetallic NP catalysts, an isolated bimetallic site supported on a nonmetallic surface could possess distinctly different catalytic properties from those of the SACs discussed above and from their bimetallic NP counterparts. The cationic state of a singly dispersed bimetallic site may provide unique features for desirable catalytic reactions. Zhang et al. synthesized isolated Rh_1Co_3 bimetallic sites on Co_3O_4 nanorods and tested these catalysts for CO reduction of NO molecules.⁸⁰ The strong adsorption of two nitric oxide molecules and a nitrous oxide intermediate on the Rh_1Co_3 sites and the available low-barrier pathway for dissociation to dinitrogen and an oxygen atom yielded a 100% selectivity for reducing NO to N_2 at 110 °C with a much higher activity than the Rh-Co bimetallic NP counterparts.⁸⁰ In this particular case, the Rh_1 atom together with the 3 Co atoms form the active center for the NO reduction reaction. This work opens the door for developing singularly dispersed bimetallic nanocluster catalysts.

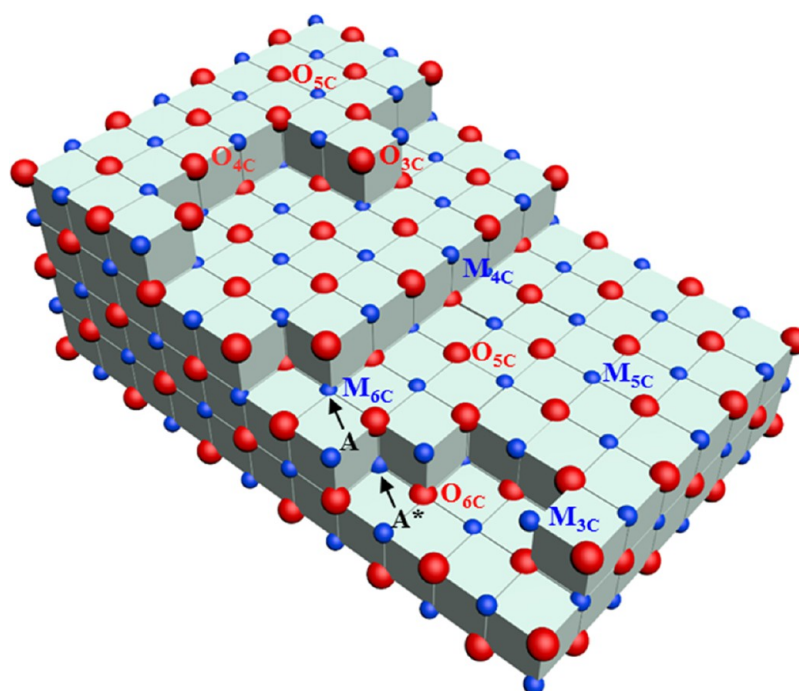


Figure 24. Schematic diagram illustrates the various sites on a metal oxide surface due to the presence of steps, kinks, corners, etc. Vacancies and other types of surface defects are not shown. The model represents metal oxides with a rock-salt crystal structure (e.g., NiO, MgO, etc.). The small blue dots represent metal cations, and the larger red dots represent oxygen anions. The label NC represents the coordination number of N .

Numerous examples reported in this Perspective clearly suggest that the single metal atoms play the most important role in determining the catalytic properties of a SAC. The interaction between the metal atom and the support atoms, however, significantly influences the catalytic behavior of the SAC. This has been clearly demonstrated by the strong interaction of metal atoms with N-doped carbons to form M_1-N-C complexes. For metal atoms supported on metal oxides, the M_1-O_{support} bonding must play a dominant role in determining the catalytic performance of the metal oxides supported metal SACs. When the surfaces of the support materials are functionalized the functional groups (e.g., OH groups, N-containing groups, S-containing groups, etc.) may play the most important role in modulating the catalytic properties of the metal SACs.

7. ANCHORING AND LOCALIZING SINGLE METAL ATOMS

From the above discussions it is clear that anchoring and localizing single metal atoms onto support surfaces are the most critical barriers to designing and developing highly efficient and stable supported metal SACs. In order to develop stable SACs, better understanding and engineering of surface defects and anchoring sites are imperative. This brings us back to focus on developing robust synthesis protocols and the ability to functionalize/engineer the support surfaces.

Many surface asperities exist on a crystalline metal oxide support. For example, Figure 24 schematically illustrates the various types of coordinately unsaturated surface atoms (cations and anions) of a divalent metal oxide with a rock-salt crystal structure. Highly unsaturated outward corner (3 dangling bonds), edge (2 dangling bonds), and face (1 dangling bond) metal cations or oxygen anions are clearly illustrated. It is interesting to note that even fully coordinated outward and inward corner cations (e.g., indicated by A and A*, respectively,

in Figure 24) or anions may be accessible by small reactant molecules or single metal atoms. The fully coordinated cation located at A possesses different environment from that located at A*. All these different types of surface atoms and surface cation or anion vacancies (cf. Figure 21) are present in a practical metal oxide support, and they will interact with the single metal atoms differently, resulting in heterogeneity of catalytically active centers in metal SACs.

If a metal atom can substitutionally replace a surface cation of a metal oxide support then the metal atom may be strongly anchored due to its interaction with the neighboring oxygen anions. We have found that with very low levels of metal loading noble metal atoms can substitutionally dope the various types of metal oxides (cf. Figure 21). The substitutionally doped metal atoms may carry a positive charge and thus influence their binding strengths for reactant molecules (e.g., CO molecules) or modulate their behavior for dissociative adsorption of H_2 or other molecules. Other approaches to anchoring single metal atoms have recently been investigated. By using a combination of photoelectron spectroscopy, STM and DFT calculations a recent report concluded that Pt single atoms on ceria are stabilized by the monatomic step edges.¹⁸⁰ Pt segregation at steps leads to stable dispersions of single Pt^{2+} ions in planar PtO_4 moieties, which incorporate excess oxygen atoms and thus contribute to oxygen storage capacity of ceria.¹⁸⁰ The authors experimentally controlled the step density of the ceria and demonstrated that step engineering and the subsequent step decoration by metal atoms represent an effective strategy for anchoring single metal atoms.¹⁸⁰

By utilizing a 2-D titania layer with periodic 6- and 10-membered nanopores of a reconstructed $SrTiO_3(110)$ surface as substrate, Wang et al. anchored Ni single adatoms onto the open pores and found that an in-gap state induced an upward band bending.¹⁸¹ Both experimental and DFT calculations suggest that the Ni adatoms are positively charged and remain

extremely stable. By anchoring Pd atoms into the cavities of mesoporous polymeric graphitic carbon nitride, Vile et al. successfully stabilized the Pd single atoms which are highly dispersed into the porous carbon nitride.⁷⁷ The isolated Pd atoms were confined within the 6-fold cavities of the mp-g-C₃N₄, thus realizing stable Pd₁ SACs for hydrogenation of alkynes and nitroarenes.

Yang et al. have demonstrated that Na and K can stabilize Au single atoms along with hydroxyl and oxo groups.⁶⁶ They have used UV-assisted methods to prepare mononuclear Au–O(OH)_x species onto titania with a loading level up to 1.2 wt %. The Au cations remained stable and active for WGS reactions from ~80° to 250 °C. They further demonstrated that by addition of Na and K ion species the Au–O(OH)_x complexes can be anchored onto inert and irreducible metal oxide supports for WGS reaction. The single-site active species share common geometric features: The –O ligands bind directly to the central Au atom; Na atoms are linked to the Au atom through the –O ligands and the OH groups are connected to the 3-fold “Na₃” sites that surround the Au atom.⁶⁶ The purpose of building such closely bound nanoclusters is to stabilize the single metal atom and in the process to modulate its electronic structure. As long as the nanoclusters as a whole provide desirable catalytic properties such a strategy is beneficial and should be broadly explored.

By employing a photochemical approach to fabricating stable supported metal SACs, Liu et al. dispersed Pd single atoms on ethylene glycolate–stabilized ultrathin TiO₂ nanosheets.⁸⁸ The Pd₁/TiO₂ SAC exhibited high catalytic activity in hydrogenation of C=C bonds, exceeding that of surface Pd atoms on commercial Pd catalysts by a factor of 9 and a catalytic enhancement in hydrogenation of aldehydes by a factor of more than 55. The UV light-induced formation of ethylene glycolate radicals on TiO₂ nanosheets was proposed to be critical for preparing the ultrastable Pd₁/TiO₂ SAC with a Pd loading as high as 1.5 wt %. Such a synthesis approach should be extended to other systems to develop stable SACs for targeted catalytic reactions.

By anchoring Pt single atoms onto the 4-fold hollow sites of phosphomolybdic acid modified active carbon, a Pt SAC was recently synthesized with a Pt loading level of about 1.0 wt %.¹⁸² Each Pt atom is stabilized by four oxygen atoms in a distorted square-planar geometry, with Pt slightly protruding from the oxygen planar surface. The resulting Pt atom is positively charged and can adsorb hydrogen easily. This catalyst has demonstrated excellent performance for hydrogenation of nitrobenzene and cyclohexanone.¹⁸²

Peterson et al., using industrially relevant γ -Al₂O₃ support doped with La, stabilized isolated Pd atoms on the γ -Al₂O₃ and used this catalyst for a low-temperature CO oxidation reaction.⁷³ The catalyst activity can be regenerated by oxidation at 700 °C in air. The high-temperature stability and regenerability of the Pd₁/ γ -Al₂O₃ SAC make this catalyst system of potential for practical applications. The stability of the Pd single atoms and the support may derive from the anchoring effects of the La dopants.

Jones et al. recently anchored Pt single atoms onto ceria nanorods by using a high-temperature vapor transport method.¹³³ The synthesized Pt₁/CeO₂ SAC is sinter-resistant and stable during CO oxidation reaction at temperatures as high as 300 °C. Synthesis of single metal atoms at high temperatures ensures that only the most stable binding sites are

occupied, yielding a sinter-resistant, atomically dispersed catalyst.

All these examples discussed above demonstrate that anchoring of supported single metal atoms can be accomplished via various types of synthesis approaches. The anchoring and localization of single metal atoms on high-surface-area supports will enable the practical applications of supported metal SACs.

8. CHALLENGES AND PROSPECTS

The fact that we can manipulate, examine, and test dispersed single metal atoms for catalysis is both intellectually exciting and stimulating. The recent discovery of catalysis by supported single metal atoms and the development of routinely accessible synthesis protocols of supported metal SACs that exhibit high catalytic activity and selectivity, as discussed in this Perspective, make it possible to consider potential industrial applications, especially since the preparation of many SACs can be accomplished by scalable synthesis. The availability of aberration-corrected STEM and EXAFS techniques makes it routinely accessible to readily discriminating single atoms from NPs and clusters. The major challenge is to find practical methods to strongly anchor single atoms of expensive metals to high-surface-area and low-cost support materials. When stable SACs with high metal loadings are achieved the commercialization of supported single metal atoms should transform many important technologies including technologies for energy generation, emission control of automobiles, water purification, and production of chemicals.

Anchoring individually isolated atoms for function is not only critical to heterogeneous catalysis but also to the nano-electronics and optoelectronics communities. For example, single-atom transistors have been constructed by anchoring a phosphorus atom to a silicon surface.¹⁸³ An individual phosphorus dopant atom can be deterministically placed within an epitaxial silicon device architecture with a spatial accuracy of one lattice site. The presence of discrete quantum levels in the energy spectrum of the anchored P atom has been confirmed. By utilizing the electron spin property of an anchored P single atom, a quantum bit (qubit), which is the basic unit of a quantum computer, has been constructed.¹⁸⁴

By securely anchoring a Ho atom onto the 4-fold symmetry position of an MgO surface single-atom memory devices have been realized.¹⁸⁵ The extraordinary stability of the Ho single atom is achieved by the realization of a symmetry-protected magnetic ground state and by decoupling the Ho spin from the underlying metal by a tunnel barrier film (MgO). These recent advances on utilizing isolated single atoms as functioning units, including catalysis by anchored single atoms, push the nanoscience and nanotechnology to the ultimate limit of single atoms.

The grand challenge in catalysis by supported single metal atoms is the strong anchoring of specific metal atoms to a suitable high-surface-area support with high number density of metal atoms. To achieve this goal, engineering and functionalizing support surfaces become critical. With the recent capability of rational designing and developing shape-controlled nanostructures or other types of complicated nanostructures,^{186,187} it is expected that breakthroughs in nanostructuring and functionalizing metal oxides and other types of support materials will significantly advance the development of practical SACs for broad technological applications.

The fact that isolated metal atoms possess high energy per atom (compared to that in the bulk metal) suggests that individual metal atoms can interact strongly with support surfaces. By manipulating the interactions of metal atoms with surface defects (high energy sites) on a support, the energy of the composite system (single metal atom plus the surrounding atoms on the support) may become a local minimum in the energy landscape of the metal–support composite system. When this occurs the metal atoms can be anchored and remain stable at high temperatures. Figure 25 demonstrates such an

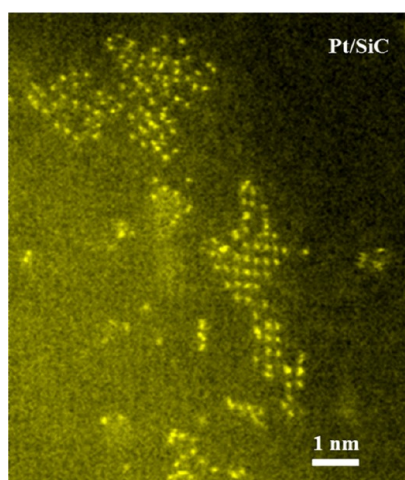


Figure 25. Aberration-corrected HAADF-STEM image of Pt atoms dispersed onto SiC substrate after high-temperature (~ 800 °C) treatment inside the electron microscope. The Pt atoms (bright dots) were strongly anchored onto the SiC surface.

example. After high-temperature (800 °C) treatment inside an electron microscope, Pt atoms were strongly anchored onto the surfaces of SiC nanocrystallites either randomly or with a superstructure. The understanding of such anchoring mechanism may help us gain insights into developing desirable support materials to anchor single metal atoms.

Transformations of nanocrystals by cation exchange in appropriate liquid solutions have been extensively used to access a wide variety of materials and nanostructures. Controlled ion exchange method can be used to produce various types of nanoscale heterostructures including core/shell type structures. Galvanic replacement reaction process has been utilized to make heterostructured metal oxide nanoshapes.¹⁸⁸ Similar approaches may be developed to deposit single metal atoms onto surfaces of nanostructured metal oxide supports. Figure 26 shows an atomic resolution image of a Pd₁/ZnO nanobelt model catalyst. The synthesis process of such model SAC catalysts include immersing the ZnO nanobelt into a solution that contains Pd ion complexes. By carefully controlling the strong electrostatic adsorption process, patches of Pd monolayers or Pd single atoms were securely anchored onto the ZnO {10–10} surfaces. Further optimization of such a synthesis process may provide a way to disperse a high number density of single metal atoms onto appropriate nanostructured metal oxide supports. High number-density Pt single atoms, dimers, or even chains have been dispersed onto FeO_x nanocrystallites via wet chemistry method (Figure 27).

Development of metal SACs should take advantage of the recent rapid advances in two-dimensional (2D) materials. With monolayer or thin-layers as supports, the dispersion and

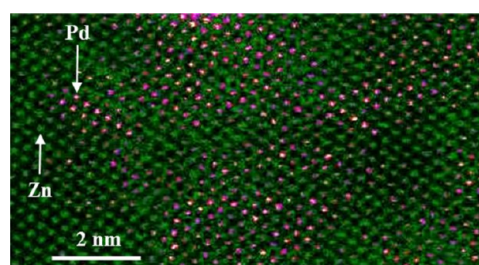


Figure 26. Aberration-corrected HAADF-STEM image of Pd atoms adsorbed onto a ZnO nanobelt clearly shows the high number density of isolated Pd atoms (bright dots). These Pd atoms seem to form patches of monolayer coverage on the ZnO {10–10} nanoscale facets.

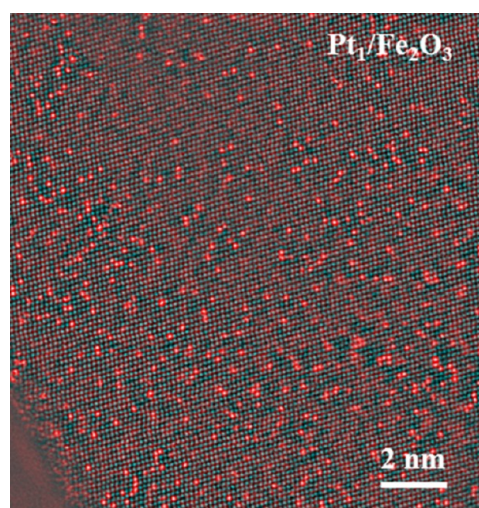


Figure 27. Processed HAADF-STEM (RGB) image of a Pt₁/Fe₂O₃ SAC clearly shows the uniform distribution of the high number density of isolated Pt atoms (bright dots) and the Fe₂O₃ lattice. The majority of the Pt single atoms are located at the Fe cation positions.

anchoring of single metal atoms should be very different because the 2D materials possess different electronic structures from those of their bulk counterparts. Therefore, the manipulation of single metal atoms on 2D supports may provide unique opportunities to tune catalytically active centers for desired catalytic reactions.

The combined use of theoretical DFT calculations with advanced characterization techniques has provided deep insights in understanding the stability of, and catalysis by, supported single metal atoms. For example, Aleksandrov et al. employed DFT calculations to predict the structure and relative stability of Pt₁ species on Ce₂₁O₄₂ nanostructures.¹⁸⁹ They found that the stability of the Pt species depends on the reduction or oxidation environment of the system. The DFT calculations suggest that the most stable Pt₁ species is Pt²⁺ coordinated in a square-planar complex with four oxygen anions as ligands on small ceria {100} facets. Even under partial reduction conditions, the Pt²⁺ species were still stable. When the Pt species were located on other positions, they maintain the metallic nature and may not be stable. Furthermore, the authors analyzed the stability of the supported Pt₁ species under various conditions. Such predictions on the location and stability of supported single metal atoms by DFT calculations should help the design of stable SACs.

Neitzel et al. investigated the stability and the reactivity of M₁ (M = Pt, Pd, and Ni) species on nanostructured CeO₂ films by

DFT calculations and spectroscopy techniques.¹⁹⁰ They found that all the M_1^{2+} species possess higher adsorption energies than their corresponding cohesive energies in the bulk metals. Unlike the Pt_1/CeO_2 system as shown by Aleksandrov et al.,¹⁸⁹ the authors found that Pd^{2+} species can be stabilized inside bulk CeO_2 . While both the Pt^{2+} and Pd^{2+} species can activate H_2 , the $Ni-CeO_2$ system does not exhibit such reactivity due to the extremely strong binding of the Ni^{2+} species. This type of prediction and understanding proves the power in utilizing DFT calculations to understand the experimentally observed phenomena and to help design better SACs.

By using ab initio molecular dynamics simulations, Wang et al. found that during CO oxidation on the Au/CeO_2 system, the adsorbed CO molecules induce a dynamic process to produce Au single atoms from the Au NPs, and these Au single atoms are highly active for CO oxidation.¹⁹¹ The reason for this to occur is that Au cations strongly couple with the redox properties of the ceria to lower the energy of the redox reactions. The Au_1 cation can break away from the Au NP and during this process catalyze CO oxidation. After the reaction is completed the Au_1 reruns back to the Au NP to complete the reaction cycle. This study highlights the importance of dynamic creation of active sites under reaction conditions and connects catalysis by single metal atoms to catalysis by the peripheral atoms of supported metal NPs.

In a most recent paper, Aleksandrov et al. calculated the stretching frequency of a CO probe molecule on atomically dispersed Pt monomers, clusters and NPs on CeO_2 support.¹⁹² The authors analyzed the effect of metal coordination number and charge on the vibrational frequencies of CO in various model systems and concluded that the shift of the vibrational frequency of the CO probe molecules depends on complicated factors. Such a molecular level understanding of the atomically dispersed metal species is clearly valuable in guiding the correct interpretation of experimental results.

It is expected that with innovative synthesis strategies, advanced characterization tools, robust kinetic studies, and theoretical calculations we can make significant progress in understanding the fundamental properties of supported single metal atoms and realize the ultimate goal of manipulating individual atoms for function. The emerging research field of supported single atoms, such as single-atom catalysis in chemistry, single-atom transistor and memory in physics/electronics, and single-atom magnetic and optoelectronic applications, permits us to deepen our understanding of the nature of the smallest building blocks and how systems are formed from the bottom up. We now are truly living in the era of "Plenty of Room at the Bottom".¹⁹³

AUTHOR INFORMATION

Corresponding Author

*E-mail: Jingyue.liu@asu.edu.

Notes

The author declares no competing financial interest.

ACKNOWLEDGMENTS

This work was funded by the National Science Foundation under CHE-1465057. The author acknowledges the use of the facilities in the John M. Cowley Center for High Resolution Electron Microscopy at Arizona State University. The author appreciates numerous discussions with Professors Tao Zhang, Aiqing Wang, and Weixue Li of the Dalian Institute of

Chemical Physics of the Chinese Academy of Sciences, Professor Jun Li of Tsinghua University, and Dr. Lawrence F. Allard of Oak Ridge National Laboratory. The author acknowledges extensive discussions with his research group members Dr. Botao Qiao, Dr. Yang Lou, Ms. Jia Xu, Dr. Sibin Duan, and Dr. Engshen Zhan. The author especially thanks Ms. Jia Xu for providing some of the illustrations used in this Perspective and Dr. Xiang-Kui Gu for discussions on modeling and DFT calculations.

REFERENCES

- (1) Heck, R. M.; Farrauto, R. J. *Appl. Catal., A* **2001**, *221*, 443–457.
- (2) Bell, A. T. *Science* **2003**, *299*, 1688–1691.
- (3) Deluga, G. A.; Salge, J. R.; Schmidt, L. D.; Verykios, X. E. *Science* **2004**, *303*, 993–997.
- (4) Chen, M. S.; Goodman, D. W. *Science* **2004**, *306*, 252–255.
- (5) Zhang, J.; Sasaki, K.; Sutter, E.; Adzic, R. R. *Science* **2007**, *315*, 220–222.
- (6) Antolini, E. *Appl. Catal., B* **2009**, *88*, 1–24.
- (7) Vajda, S.; Pellin, M. J.; Greeley, J. P.; Marshall, C. L.; Curtiss, L. A.; Ballentine, G. A.; Elam, J. W.; Catillon-Mucherie, S.; Redfern, P. C.; Mehmood, F.; Zapol, P. *Nat. Mater.* **2009**, *8*, 213–216.
- (8) Ma, Z.; Dai, S. *ACS Catal.* **2011**, *1*, 805–818.
- (9) Van Hardeveld, R.; Hartog, F. *Surf. Sci.* **1969**, *15*, 189–230.
- (10) Gates, B. C. *Chem. Rev.* **1995**, *95*, 511–522.
- (11) Lopez, N.; Janssens, T. V. W.; Clausen, B. S.; Xu, Y.; Mavrikakis, M.; Bligaard, T.; Nørskov, J. K. *J. Catal.* **2004**, *223*, 232–235.
- (12) Cuenya, B. R. *Thin Solid Films* **2010**, *518*, 3127–3150.
- (13) Kubo, R. *J. Phys. Soc. Jpn.* **1962**, *17*, 975–986.
- (14) Johansson, M. P.; Sundholm, D.; Vaara, J. *Angew. Chem.* **2004**, *116*, 2732–2735.
- (15) von Issendorff, B.; Cheshnovsky, O. *Annu. Rev. Phys. Chem.* **2005**, *56*, 549–580.
- (16) Roduner, E. *Chem. Soc. Rev.* **2006**, *35*, 583–592.
- (17) Valden, M.; Lai, X.; Goodman, D. W. *Science* **1998**, *281*, 1647–1650.
- (18) Claus, P.; Brückner, A.; Mohr, C.; Hofmeister, H. *J. Am. Chem. Soc.* **2000**, *122*, 11430–11439.
- (19) Li, J.; Li, X.; Zhai, H. J.; Wang, L. S. *Science* **2003**, *299*, 864–867.
- (20) Haruta, M. *Catal. Today* **1997**, *36*, 153–166.
- (21) Yoon, B.; Häkkinen, H.; Landman, U.; Wörz, A. S.; Antonietti, J.-M.; Abbet, S.; Judai, K.; Heiz, U. *Science* **2005**, *307*, 403–407.
- (22) Tauster, S. J.; Fung, S. C.; Baker, R. T. K.; Horsley, J. A. *Science* **1981**, *211*, 1121–1125.
- (23) Campbell, C. T. *Surf. Sci. Rep.* **1997**, *27*, 1–111.
- (24) Fu, Q.; Wagner, T. *Surf. Sci. Rep.* **2007**, *62*, 431–498.
- (25) Liu, J. *ChemCatChem* **2011**, *3*, 934–948.
- (26) Haruta, M.; Kobayashi, T.; Sano, H.; Yamada, N. *Chem. Lett.* **1987**, *16*, 405–408.
- (27) Xu, Z.; Xiao, F.-S.; Purnell, S. K.; Alexeev, O.; Kawi, S.; Deutsch, S. E.; Gates, B. C. *Nature* **1994**, *372*, 346–348.
- (28) Heiz, U.; Sanchez, A.; Abbet, S.; Schneider, W.-D. *J. Am. Chem. Soc.* **1999**, *121*, 3214–3217.
- (29) Somorjai, G. A.; Park, J. Y. *Chem. Soc. Rev.* **2008**, *37*, 2155–2162.
- (30) Crespo-Quesada, M.; Yarulin, A.; Jin, M.; Xia, Y.; Kiwi-Minsker, L. *J. Am. Chem. Soc.* **2011**, *133*, 12787–12794.
- (31) Schmidt, M.; Kusche, R.; Hippler, T.; Donges, J.; Kronmüller, W.; von Issendorff, B.; Haberland, H. *Phys. Rev. Lett.* **2001**, *86*, 1191–1194.
- (32) Taylor, S.; Lemire, G. W.; Hamrick, Y. M.; Fu, Z.; Morse, M. D. *J. Chem. Phys.* **1988**, *89*, 5517–5523.
- (33) Lei, Y.; Mehmood, F.; Lee, S.; Greeley, J.; Lee, B.; Seifert, S.; Winans, R. E.; Elam, J. W.; Meyer, R. J.; Redfern, P. C.; Teschner, D.; Schlögl, R.; Pellin, M. J.; Curtiss, L. A.; Vajda, S. *Science* **2010**, *328*, 224–228.
- (34) Hao, Y.; Gates, B. C. *J. Catal.* **2009**, *263*, 83–91.

- (35) Turner, M.; Golovko, V. B.; Vaughan, O. P. H.; Abdulkin, P.; Berenguer-Murcia, A.; Tikhov, M. S.; Johnson, B. F. G.; Lambert, R. M. *Nature* **2008**, *454*, 981–983.
- (36) Kaden, W. E.; Wu, T.; Kunkel, W. A.; Anderson, S. L. *Science* **2009**, *326*, 826–829.
- (37) Vajda, S.; White, M. G. *ACS Catal.* **2015**, *5*, 7152–7176.
- (38) Tyo, E. C.; Vajda, S. *Nat. Nanotechnol.* **2015**, *10*, 577–588.
- (39) Li, G.; Jin, R. *Acc. Chem. Res.* **2013**, *46*, 1749–1758.
- (40) Qiao, B.; Wang, A.; Yang, X.; Allard, L. F.; Jiang, Z.; Cui, Y.; Liu, J.; Li, J.; Zhang, T. *Nat. Chem.* **2011**, *3*, 634–641.
- (41) Yang, X.-F.; Wang, A.; Qiao, B.; Li, J.; Liu, J.; Zhang, T. *Acc. Chem. Res.* **2013**, *46*, 1740–1748.
- (42) Thomas, J. M.; Raja, R.; Lewis, D. W. *Angew. Chem., Int. Ed.* **2005**, *44*, 6456–6482.
- (43) Thomas, J. M. *Phys. Chem. Chem. Phys.* **2014**, *16*, 7647–7661.
- (44) Pelletier, J. D. A.; Basset, J.-M. *Acc. Chem. Res.* **2016**, *49*, 664–677.
- (45) Abbet, S.; Sanchez, A.; Heiz, U.; Schneider, W. D.; Ferrari, A. M.; Pacchioni, G.; Rösch, N. *J. Am. Chem. Soc.* **2000**, *122*, 3453–3457.
- (46) Fu, Q.; Saltsburg, H.; Flytzani-Stephanopoulos, M. *Science* **2003**, *301*, 935–938.
- (47) Zhang, X.; Shi, H.; Xu, B. Q. *Angew. Chem., Int. Ed.* **2005**, *44*, 7132–7135.
- (48) Hackett, S. F.; Brydson, R. M.; Gass, M. H.; Harvey, I.; Newman, A. D.; Wilson, K.; Lee, A. F. *Angew. Chem., Int. Ed.* **2007**, *46*, 8593–8596.
- (49) Zhai, Y.; Pierre, D.; Si, R.; Deng, W.; Ferrin, P.; Nilekar, A. U.; Peng, G.; Herron, J. A.; Bell, D. C.; Saltsburg, H.; Mavrikakis, M.; Flytzani-Stephanopoulos, M. *Science* **2010**, *329*, 1633–1636.
- (50) Wang, G.; Su, J.; Gong, Y.; Zhou, M.; Li, J. *Angew. Chem., Int. Ed.* **2010**, *49*, 1302–1305.
- (51) Jirkovsky, J. S.; Panas, I.; Ahlberg, E.; Halasa, M.; Romani, S.; Schiffrin, D. J. *J. Am. Chem. Soc.* **2011**, *133*, 19432–19441.
- (52) Kyriakou, G.; Boucher, M. W.; Jewell, A. D.; Lewis, E. A.; Lawton, T. J.; Baber, A. E.; Tierney, H. L.; Flytzani-Stephanopoulos, M.; Sykes, E. C. *Science* **2012**, *335*, 1209–1212.
- (53) Ranocchiaro, M.; Lothschütz, C.; Grolimund, D.; van Bokhoven, J. A. *Proc. R. Soc. London, Ser. A* **2012**, *468*, 1985–1999.
- (54) Flytzani-Stephanopoulos, M.; Gates, B. C. *Annu. Rev. Chem. Biomol. Eng.* **2012**, *3*, 545–574.
- (55) Lu, J.; Aydin, C.; Browning, N. D.; Gates, B. C. *Angew. Chem., Int. Ed.* **2012**, *51*, 5842–5846.
- (56) Zhang, H.; Watanabe, T.; Okumura, M.; Haruta, M.; Toshima, N. *Nat. Mater.* **2012**, *11*, 49–52.
- (57) Novotný, Z.; Argentero, G.; Wang, Z.; Schmid, M.; Diebold, U.; Parkinson, G. *Phys. Rev. Lett.* **2012**, *108*, 216103.
- (58) Bayram, E.; Lu, J.; Aydin, C.; Uzun, A.; Browning, N. D.; Gates, B. C.; Finke, R. G. *ACS Catal.* **2012**, *2*, 1947–1957.
- (59) Huang, Z.; Gu, X.; Cao, Q.; Hu, P.; Hao, J.; Li, J.; Tang, X. *Angew. Chem., Int. Ed.* **2012**, *51*, 4198–4203.
- (60) Lin, J.; Wang, A. Q.; Qiao, B. T.; Liu, X. Y.; Yang, X. F.; Wang, X. D.; Liang, J. X.; Li, J.; Liu, J. Y.; Zhang, T. *J. Am. Chem. Soc.* **2013**, *135*, 15314–15317.
- (61) Yang, M.; Allard, L. F.; Flytzani-Stephanopoulos, M. *J. Am. Chem. Soc.* **2013**, *135*, 3768–3771.
- (62) Sun, S.; Zhang, G.; Gauquelin, N.; Chen, N.; Zhou, J.; Yang, S.; Chen, W.; Meng, X.; Geng, D.; Banis, M. N.; Li, R.; Ye, S.; Knights, S.; Botton, G. A.; Sham, T. K.; Sun, X. *Sci. Rep.* **2013**, *3*, 1775.
- (63) Wang, L.; Zhang, S.; Zhu, Y.; Patlolla, A.; Shan, J.; Yoshida, H.; Takeda, S.; Frenkel, A. I.; Tao, F. *ACS Catal.* **2013**, *3*, 1011–1019.
- (64) Boucher, M. B.; Zugic, B.; Cladaras, G.; Kammert, J.; Marcinkowski, M. D.; Lawton, T. J.; Sykes, E. C. H.; Flytzani-Stephanopoulos, M. *Phys. Chem. Chem. Phys.* **2013**, *15*, 12187–12196.
- (65) Wei, H.; Liu, X. Y.; Wang, A.; Zhang, L.; Qiao, B. T.; Yang, Y. F.; Huang, Y. Q.; Miao, S.; Liu, J.; Zhang, T. *Nat. Commun.* **2014**, *5*, 5634.
- (66) Yang, M.; Li, S.; Wang, Y.; Herron, J. A.; Xu, Y.; Mavrikakis, M.; Allard, L. F.; Lee, S.; Huang, J.; Flytzani-Stephanopoulos, M. *Science* **2014**, *346*, 1498–1501.
- (67) Flytzani-Stephanopoulos, M. *Acc. Chem. Res.* **2014**, *47*, 783–792.
- (68) Gu, X.-K.; Qiao, B.; Huang, C.-Q.; Ding, W.-C.; Sun, K.; Zhan, E.; Zhang, T.; Liu, J.; Li, W.-X. *ACS Catal.* **2014**, *4*, 3886–3890.
- (69) Liang, J. X.; Lin, J.; Yang, X. F.; Wang, A. Q.; Qiao, B. T.; Liu, J.; Zhang, T.; Li, J. *J. Phys. Chem. C* **2014**, *118*, 21945–21951.
- (70) Shi, Y.; Zhao, C.; Wei, H.; Guo, J.; Liang, S.; Wang, A.; Zhang, T.; Liu, J.; Ma, T. *Adv. Mater.* **2014**, *26*, 8147–8153.
- (71) Kistler, J. D.; Chotigkrai, N.; Xu, P.; Enderle, B.; Praserthdam, P.; Chen, C. Y.; Browning, N. D.; Gates, B. C. *Angew. Chem., Int. Ed.* **2014**, *53*, 8904–8907.
- (72) Guo, X. G.; Fang, G. Z.; Li, G.; Ma, H.; Fan, H. J.; Yu, L.; Ma, C.; Wu, X.; Deng, D. H.; Wei, M. M.; Tan, D.; Si, R.; Zhang, S.; Li, J. Q.; Sun, L. T.; Tang, Z. C.; Pan, X. L.; Bao, X. H. *Science* **2014**, *344*, 616–619.
- (73) Peterson, E. J.; DeLaRiva, A. T.; Lin, S.; Johnson, R. S.; Guo, H.; Miller, J. T.; Kwak, J. H.; Peden, C. H. F.; Kiefer, B.; Allard, L. F.; Ribeiro, F. H.; Datye, A. K. *Nat. Commun.* **2014**, *5*, 4885.
- (74) Duarte, R. B.; Krumeich, F.; van Bokhoven, J. A. *ACS Catal.* **2014**, *4*, 1279–1286.
- (75) Zugic, B.; Zhang, S.; Bell, D. C.; Tao, F.; Flytzani-Stephanopoulos, M. *J. Am. Chem. Soc.* **2014**, *136*, 3238–3245.
- (76) Qiao, B.; Liang, J.-X.; Wang, A.; Xu, C.-Q.; Li, J.; Zhang, T.; Liu, J. *Nano Res.* **2015**, *8*, 2913–2924.
- (77) Vilé, G.; Albani, D.; Nachtegaal, M.; Chen, Z.; Dontsova, D.; Antonietti, M.; López, N.; Pérez-Ramírez, J. *Angew. Chem., Int. Ed.* **2015**, *54*, 11265–11269.
- (78) Fei, H.; Dong, J.; Arellano-Jimenez, M. J.; Ye, G.; Dong Kim, N.; Samuel, E. L.; Peng, Z.; Zhu, Z.; Qin, F.; Bao, J.; Yacaman, M. J.; Ajayan, P. M.; Chen, D.; Tour, J. M. *Nat. Commun.* **2015**, *6*, 8668.
- (79) Yang, M.; Liu, J.; Lee, S.; Zugic, B.; Huang, J.; Allard, L. F.; Flytzani-Stephanopoulos, M. *J. Am. Chem. Soc.* **2015**, *137*, 3470–3473.
- (80) Zhang, S.; Nguyen, L.; Liang, X.-J.; Shan, J.; Liu, J.; Frenkel, A. I.; Patlolla, A.; Huang, W.; Li, J.; Tao, F. *Nat. Commun.* **2015**, *6*, ArticleNo. 7938.
- (81) Zhang, L.; Wang, A.; Wang, W.; Huang, Y.; Liu, X.; Miao, S.; Liu, J.; Zhang, T. *ACS Catal.* **2015**, *5*, 6563–6572.
- (82) Qiao, B.; Liu, J.; Wang, Y.-G.; Lin, Q.; Liu, X.; Wang, A.; Li, J.; Zhang, T.; Liu, J. *ACS Catal.* **2015**, *5*, 6249–6254.
- (83) Lin, J.; Qiao, B.; Li, N.; Li, L.; Sun, X.; Liu, J.; Wang, X.; Zhang, T. *Chem. Commun.* **2015**, *51*, 7911–7914.
- (84) Jiang, M.; Yan, L.; Ding, Y.; Sun, Q.; Liu, J.; Zhu, H.; Lin, R.; Xiao, F.; Jiang, Z.; Liu, J. *J. Mol. Catal. A: Chem.* **2015**, *404–405*, 211–217.
- (85) Qiao, B.; Lin, J.; Wang, A.; Chen, Y.; Zhang, T.; Liu, J. *Chin. J. Catal.* **2015**, *36*, 1505–1511.
- (86) Dvořák, F.; Camellone, M. F.; Tovt, A.; Tran, N.-D.; Negreiros, F. R.; Vorokhta, M.; Skála, T.; Matolínová, I.; Mysliveček, J.; Matolín, V.; Fabris, S. *Nat. Commun.* **2016**, *7*, 10801.
- (87) Liu, J.; Lucci, F. R.; Yang, M.; Lee, S.; Marcinkowski, M. D.; Therrien, A. J.; Williams, C. T.; Sykes, E. C. H.; Flytzani-Stephanopoulos, M. *J. Am. Chem. Soc.* **2016**, *138*, 6396–6399.
- (88) Liu, P.; Zhao, Y.; Qin, R.; Mo, S.; Chen, G.; Gu, L.; Chevrier, D. M.; Zhang, P.; Guo, Q.; Zang, D.; Wu, B.; Fu, G.; Zheng, N. *Science* **2016**, *352*, 797–800.
- (89) Li, X.; Bi, W.; Zhang, L.; Tao, S.; Chu, W.; Zhang, Q.; Luo, Y.; Wu, C.; Xie, Y. *Adv. Mater.* **2016**, *28*, 2427–2431.
- (90) Fan, L.; Liu, P. F.; Yan, X.; Gu, L.; Yang, Z. Z.; Yang, H. G.; Qiu, S.; Yao, X. *Nat. Commun.* **2016**, *7*, ArticleNo. 10667.
- (91) Chen, Y.; Huang, Z.; Hu, P.; Chen, J.; Tang, X. *Catal. Commun.* **2016**, *75*, 74–77.
- (92) Zhang, R. Q.; Lee, T. H.; Yu, B. D.; Stampfl, C.; Soon, A. *Phys. Chem. Chem. Phys.* **2012**, *14*, 16552–16557.
- (93) Sen, F. G.; Qi, Y.; Alpas, A. T. *J. Phys.: Condens. Matter* **2012**, *24*, 225003.
- (94) Poh, C. K.; Lim, S. H.; Lin, J. Y.; Feng, Y. P. *J. Phys. Chem. C* **2014**, *118*, 13525–13538.
- (95) Ding, W. C.; Gu, X. K.; Su, H. Y.; Li, W. X. *J. Phys. Chem. C* **2014**, *118*, 12216–12223.

- (96) Hu, P. P.; Huang, Z. W.; Amghouz, Z.; Makkee, M.; Xu, F.; Kapteijn, F.; Dikhtiarenko, A.; Chen, Y. X.; Gu, X.; Tang, X. F. *Angew. Chem., Int. Ed.* **2014**, *53*, 3418–3421.
- (97) Li, F.; Li, Y.; Zeng, X. C.; Chen, Z. *ACS Catal.* **2015**, *5*, 544–552.
- (98) Gao, G.; Jiao, Y.; Waclawik, E. R.; Du, A. J. *Am. Chem. Soc.* **2016**, *138*, 6292–6297.
- (99) Liu, X.; Yang, Y.; Chu, M.; Duan, T.; Meng, C.; Han, Y. *Catal. Sci. Technol.* **2016**, *6*, 1632–1641.
- (100) Corma, A. *J. Catal.* **2003**, *216*, 298–312.
- (101) Corma, A.; García, H.; Llabrés i Xamena, F. X. *Chem. Rev.* **2010**, *110*, 4606–4655.
- (102) Ehresmann, J. O.; Kletnieks, P. W.; Liang, A.; Bhirud, V. A.; Bagatchenko, O. P.; Lee, E. J.; Klaric, M.; Gates, B. C.; Haw, J. F. *Angew. Chem., Int. Ed.* **2006**, *45*, 574–576.
- (103) Uzun, A.; Bhirud, V. A.; Kletnieks, P. W.; Haw, J. F.; Gates, B. C. *J. Phys. Chem. C* **2007**, *111*, 15064–15073.
- (104) Ortalan, V.; Uzun, A.; Gates, B. C.; Browning, N. D. *Nat. Nanotechnol.* **2010**, *5*, 506–510.
- (105) Serna, P.; Gates, B. C. *J. Am. Chem. Soc.* **2011**, *133*, 4714–4717.
- (106) Lu, J.; Aydin, C.; Browning, N. D.; Gates, B. C. *Angew. Chem.* **2012**, *124*, 5944–5948.
- (107) Serna, P.; Gates, B. C. *Acc. Chem. Res.* **2014**, *47*, 2612–2620.
- (108) Martínez-Macias, C.; Serna, P.; Gates, B. C. *ACS Catal.* **2015**, *5*, 5647–5656.
- (109) Narula, C. K.; Moses-DeBusk, M. Catalysis on Single Supported Atoms. In *Catalysis by Materials with Well-Defined Structures*; Wu, Z. L., Overbury, S. H., Eds.; Elsevier Science: Amsterdam, 2015; pp 263–274.
- (110) McKittrick, M. W.; Jones, C. W. *J. Am. Chem. Soc.* **2004**, *126*, 3052–3053.
- (111) Tada, M.; Muratsugu, S. Site-Isolated Heterogeneous Catalysts. In *Heterogeneous Catalysts for Clean Technology: Spectroscopy, Design, and Monitoring*; Wilson, K., Lee, A. F., Eds.; Wiley-VCH Verlag GmbH & Co. KGaA: Weinheim, 2013; pp 173–191.
- (112) Copéret, C.; Comas-Vives, A.; Conley, M. P.; Estes, D. P.; Fedorov, A.; Mougél, V.; Nagae, H.; Núñez-Zarur, F.; Zhizhko, P. A. *Chem. Rev.* **2016**, *116*, 323–421.
- (113) Fu, Q.; Deng, W.; Saltsburg, H.; Flytzani-Stephanopoulos, M. *Appl. Catal., B* **2005**, *56*, 57–68.
- (114) Schwarz, J. A.; Contescu, C.; Contescu, A. *Chem. Rev.* **1995**, *95*, 477–510.
- (115) Pinna, F. *Catal. Today* **1998**, *41*, 129–137.
- (116) Kim, Y. T.; Ohshima, K.; Higashimine, K.; Uruga, T.; Takata, M.; Suematsu, H.; Mitani, T. *Angew. Chem.* **2006**, *118*, 421–425.
- (117) Brunelle, J. P. *Pure Appl. Chem.* **1978**, *50*, 1211–1229.
- (118) Regalbuto, J. R.; Agashe, K.; Navada, A.; Bricker, M. L.; Chen, Q. *Stud. Surf. Sci. Catal.* **1998**, *118*, 147–156.
- (119) Regalbuto, J. R.; Navada, A.; Shadid, S.; Bricker, M. L.; Chen, Q. *J. Catal.* **1999**, *184*, 335–348.
- (120) Jiao, L.; Regalbuto, J. R. *J. Catal.* **2008**, *260*, 329–341.
- (121) Suntola, T.; Antson, J. U.S. Patent US4058430 A, 1977.
- (122) Aleskovsky, V.; Koltcov, M. USSR Patent USSR422446, 1972.
- (123) O'Neill, B. J.; Jackson, D. H. K.; Lee, J.; Canlas, C.; Stair, P. C.; Marshall, C. L.; Elam, J. M.; Kuech, T. F.; Dumesic, J. A.; Huber, G. W. *ACS Catal.* **2015**, *5*, 1804–1825.
- (124) Guzman, J.; Gates, B. C. *Dalton Trans.* **2003**, *17*, 3303–3318.
- (125) Basset, J. M.; Lefebvre, F.; Santini, C. *Coord. Chem. Rev.* **1998**, *178–180*, 1703–1723.
- (126) Telychko, M.; Mutombo, P.; Ondráček, M.; Hapala, P.; Bocquet, F. C.; Kolorenč, J.; Vondráček, M.; Jelínek, P.; Švec, M. *ACS Nano* **2014**, *8*, 7318–7324.
- (127) Li, X. N.; Yuan, Z.; He, S. G. *J. Am. Chem. Soc.* **2014**, *136*, 3617–3623.
- (128) Li, Z. Y.; Yuan, Z.; Li, X. N.; Zhao, Y. X.; He, S. G. *J. Am. Chem. Soc.* **2014**, *136*, 14307–14313.
- (129) Zhao, Y. X.; Li, Z. Y.; Yuan, Z.; Li, X. N.; He, S. G. *Angew. Chem., Int. Ed.* **2014**, *53*, 9482–9486.
- (130) Schwarz, H. *Angew. Chem., Int. Ed.* **2015**, *54*, 10090–10100.
- (131) Patil, K. C.; Aruna, S. T.; Ekambaram, S. *Curr. Opin. Solid State Mater. Sci.* **1997**, *2*, 158–165.
- (132) Hegde, M. S.; Madras, G.; Patil, K. C. *Acc. Chem. Res.* **2009**, *42*, 704–712.
- (133) Jones, J.; Xiong, H.; DeLaRiva, A. T.; Peterson, E. J.; Pham, H.; Challa, S. R.; Qi, G.; Oh, S.; Wiebenga, M. H.; Hernández, X. I. P.; Wang, Y.; Datye, A. K. *Science* **2016**, *353*, 150–154.
- (134) Matsubu, J. C.; Yang, Y. N.; Christopher, P. *J. Am. Chem. Soc.* **2015**, *137*, 3076–3084.
- (135) Kale, M. J.; Christopher, P. *ACS Catal.* **2016**, *6*, 5599–5609.
- (136) Zhao, L.; He, R.; Rim, K. T.; Schiros, T.; Kim, K. S.; Zhou, H.; Gutiérrez, C.; Chockalingam, S. P.; Arguello, C. J.; Pálková, L.; et al. *Science* **2011**, *333*, 999–1003.
- (137) Zhou, W.; Kapetanakis, M.; Prange, M.; Pantelides, S.; Pennycook, S.; Idrobo, J.-C. *Phys. Rev. Lett.* **2012**, *109*, 206803.
- (138) Warner, J. H.; Lin, Y. C.; He, K.; Koshino, M.; Suenaga, K. *ACS Nano* **2014**, *8*, 11806–11815.
- (139) Gregor, R. B.; Lytle, F. W. *J. Catal.* **1980**, *63*, 476–486.
- (140) Alexeev, O.; Gates, B. C. *Top. Catal.* **2000**, *10*, 273–293.
- (141) Heald, S. M. *J. Synchrotron Radiat.* **2015**, *22*, 436–445.
- (142) Ryczkowski, J. *Catal. Today* **2001**, *68*, 263–381.
- (143) Lamberti, C.; Zecchina, A.; Groppo, E.; Bordiga, S. *Chem. Soc. Rev.* **2010**, *39*, 4951–5001.
- (144) Yates, Y., Jr.; Worley, T. S. D.; Duncan, T. M.; Vaughan, R. W. *J. Chem. Phys.* **1979**, *70*, 1225–1230.
- (145) Zholobenko, V. L.; Lei, G. D.; Carvill, B. T.; Lerner, B. A.; Sachler, W. M. H. *J. Chem. Soc., Faraday Trans.* **1994**, *90*, 233–238.
- (146) Ding, K.; Gulec, A.; Johnson, A. M.; Schweitzer, N. M.; Stucky, G. D.; Marks, L. D.; Stair, P. C. *Science* **2015**, *350*, 189–192.
- (147) Zhang, W.; Xu, S.; Han, X.; Bao, X. *Chem. Soc. Rev.* **2012**, *41*, 192–210.
- (148) Kwak, J. H.; Hu, J.; Mei, D.; Yi, C. W.; Kim, D. H.; Peden, C. H.; Allard, L. F.; Szanyi, J. *Science* **2009**, *325*, 1670–1673.
- (149) Corma, A.; Salnikov, O. G.; Barskiy, D. A.; Kovtunov, K. V.; Koptuyg, I. V. *Chem. - Eur. J.* **2015**, *21*, 7012–7015.
- (150) Hackett, S. F.; Brydson, R. M.; Gass, M. H.; Harvey, I.; Newman, A. D.; Wilson, K.; Lee, A. F. *Angew. Chem., Int. Ed.* **2007**, *46*, 8593–8596.
- (151) Zhang, C.; Liu, F.; Zhai, Y.; Ariga, H.; Yi, N.; Liu, Y.; Asakura, K.; Flytzani-Stephanopoulos, M.; He, H. *Angew. Chem., Int. Ed.* **2012**, *51*, 9628–9632.
- (152) Tang, W.; Hu, Z.; Wang, M.; Stucky, G. D.; Metiu, H.; McFarland, E. W. *J. Catal.* **2010**, *273*, 125–137.
- (153) Deng, D.; Chen, X.; Yu, L.; Wu, X.; Liu, Q.; Liu, Y.; Yang, H.; Tian, H.; Hu, Y.; Du, P.; Si, R.; Wang, J.; Cui, X.; Li, H.; Xiao, J.; Xu, T.; Deng, J.; Yang, F.; Duchesne, P. N.; Zhang, P.; Zhou, J.; Sun, L.; Li, J.; Pan, X.; Bao, X. *Sci. Adv.* **2015**, *1*, e1500462.
- (154) Moses-DeBusk, M.; Yoon, M.; Allard, L.; Mullins, D.; Wu, Z.; Yang, X.; Veith, G.; Stocks, G.; Narula, C. K. *J. Am. Chem. Soc.* **2013**, *135*, 12634–12645.
- (155) Yang, S.; Lee, H. *ACS Catal.* **2013**, *3*, 437–443.
- (156) Yang, S.; Kim, J.; Tak, Y. J.; Soon, A.; Lee, H. *Angew. Chem., Int. Ed.* **2016**, *55*, 2058–2062.
- (157) Lucci, F. R.; Liu, J.; Marcinkowski, M. D.; Yang, M.; Allard, L. F.; Flytzani-Stephanopoulos, M.; Sykes, E. C. H. *Nat. Commun.* **2015**, *6*, 8550.
- (158) Thomas, J. M. *Nature* **2015**, *525*, 325–326.
- (159) Siahrostami, S.; Verdaguier-Casadevall, A.; Karamad, M.; Deiana, D.; Malacrida, P.; Wickman, B.; Escudero-Escribano, M.; Paoli, E. A.; Frydendal, R.; Hansen, T. W.; Chorkendorff, I.; Stephens, I. E. L.; Rossmel, J. *Nat. Mater.* **2013**, *12*, 1137–1143.
- (160) Choi, C. H.; Kim, M.; Kwon, H. C.; Cho, S. J.; Yun, S.; Kim, H. T.; Mayrhofer, K. J. J.; Kim, H.; Choi, M. *Nat. Commun.* **2016**, *7*, 10922.
- (161) Zhang, X.; Guo, J.; Guan, P.; Liu, C.; Huang, H.; Xue, F.; Dong, X.; Pennycook, S. J.; Chisholm, M. F. *Nat. Commun.* **2013**, *4*, 1924.

- (162) Zitolo, A.; Goellner, V.; Armel, V.; Sougrati, M. T.; Mineva, T.; Stevano, L.; Fonda, E.; Jaouen, F. *Nat. Mater.* **2015**, *14*, 937–942.
- (163) Jia, Q.; Ramaswamy, N.; Hafiz, H.; Tylus, U.; Strickland, K.; Wu, G.; Barbiellini, B.; Bansil, A.; Holby, E. F.; Zelenay, P.; Mukerjee, S. *ACS Nano* **2015**, *9*, 12496–12505.
- (164) Zhang, L.; Wang, A.; Wang, W.; Huang, Y.; Liu, X.; Miao, S.; Liu, J.; Zhang, T. *ACS Catal.* **2015**, *5*, 6563–6572.
- (165) Bulushev, D. A.; Zacharska, M.; Lisitsyn, A. S.; Podyacheva, O. Y.; Hage, F. S.; Ramasse, Q. M.; Bangert, U.; Bulusheva, L. G. *ACS Catal.* **2016**, *6*, 3442–3451.
- (166) Taylor, H. S. *Proc. R. Soc. London, Ser. A* **1925**, *108*, 105–111.
- (167) Che, M. *Catal. Today* **2013**, *218–219*, 162–171.
- (168) Rim, K. T.; Eom, D.; Liu, L.; Stolyarova, E.; Raitano, J. M.; Chan, S. W.; Flytzani-Stephanopoulos, M.; Flynn, G. W. *J. Phys. Chem. C* **2009**, *113*, 10198–10205.
- (169) Ghosh, T. K.; Nair, N. N. *ChemCatChem* **2013**, *5*, 1811–1821.
- (170) Wang, H.; Feng, Q.; Cheng, Y.; Yao, Y.; Wang, Q.; Li, K.; Schwingenschlögl, U.; Zhang, X. X.; Yang, W. *J. Phys. Chem. C* **2013**, *117*, 4632–4638.
- (171) Tang, Y.; Yang, Z.; Dai, X. *Phys. Chem. Chem. Phys.* **2012**, *14*, 16566–16572.
- (172) Pala, R. G. S.; Metiu, H. *J. Phys. Chem. C* **2007**, *111*, 12715–12722.
- (173) Nolan, M.; Verdugo, V. S.; Metiu, H. *Surf. Sci.* **2008**, *602*, 2734–2742.
- (174) Li, B.; Metiu, H. *J. Phys. Chem. C* **2010**, *114*, 12234–12244.
- (175) Chrétien, S.; Metiu, H. *J. Phys. Chem. C* **2011**, *115*, 4696–4705.
- (176) Hu, Z. P.; Li, B.; Sun, X.; Metiu, H. *J. Phys. Chem. C* **2011**, *115*, 3065–3073.
- (177) Metiu, H.; Chrétien, S.; Hu, Z.; Li, B.; Sun, X. *J. Phys. Chem. C* **2012**, *116*, 10439–10450.
- (178) McFarland, E. W.; Metiu, H. *Chem. Rev.* **2013**, *113*, 4391–4427.
- (179) Nilius, N.; Freund, H.-J. *Acc. Chem. Res.* **2015**, *48*, 1532–1539.
- (180) Dvořák, F.; Farnesi Camellone, M.; Tovt, A.; Tran, N.-D.; Negreiros, F. R.; Vorokhta, M.; Skála, T.; Matolínová, I.; Mysliveček, J.; Matolín, V.; Fabris, S. *Nat. Commun.* **2016**, *7*, 10801.
- (181) Wang, Z.; Hao, X.; Gerhold, S.; Mares, P.; Wagner, M.; Bliem, R.; Schulte, K.; Schmid, M.; Franchini, C.; Diebold, U. *J. Phys. Chem. C* **2014**, *118*, 19904–19909.
- (182) Zhang, B.; Asakura, H.; Zhang, J.; Zhang, J.; De, S.; Yan, N. *Angew. Chem., Int. Ed.* **2016**, *55*, 8319–8323.
- (183) Fuechsle, M.; Miwa, J. A.; Mahapatra, S.; Ryu, H.; Lee, S.; Warschkow, O.; Hollenberg, L. C. L.; Klimeck, G.; Simmons, M. Y. *Nat. Nanotechnol.* **2012**, *7*, 242–246.
- (184) Pla, J. J.; Tan, K. Y.; Dehollain, J. P.; Lim, W. H.; Morton, J. J. L.; Jamieson, D. N.; Dzurak, A. S.; Morello, A. *Nature* **2012**, *489*, 541–545.
- (185) Donati, F.; Rusponi, S.; Stepanow, S.; Wäckerlin, C.; Singha, A.; Persichetti, L.; Baltic, R.; Diller, K.; Patthey, F.; Fernandes, E.; Dreiser, J.; Šljivančanin, Z.; Kummer, K.; Nistor, C.; Gambardella, P.; Brune, H. *Science* **2016**, *352*, 318–321.
- (186) Xia, Y.; Xia, X.; Peng, H.-C. *J. Am. Chem. Soc.* **2015**, *137*, 7947–7866.
- (187) Zhang, L.; Roling, L. T.; Wang, X.; Vara, M.; Chi, M. F.; Liu, J. Y.; Choi, S.; Park, J.; Herron, J. A.; Xie, Z. X.; Mavrikakis, M.; Xia, Y. N. *Science* **2015**, *349*, 412–416.
- (188) Oh, M. H.; Yu, T.; Yu, S. H.; Lim, B.; Ko, K. T.; Willinger, M. G.; Seo, D. H.; Kim, B. H.; Cho, M. G.; Park, J. H.; Kang, K.; Sung, Y. E.; Pinna, N.; Hyeon, T. *Science* **2013**, *340*, 964–968.
- (189) Aleksandrov, H. A.; Neyman, K. M.; Vayssilov, G. N. *Phys. Chem. Chem. Phys.* **2015**, *17*, 14551–14560.
- (190) Neitzel, A.; Figueroba, A.; Lykhach, Y.; Skála, T.; Vorokhta, M.; Tsud, N.; Mehl, S.; Ševčíková, K.; Prince, K. C.; Neyman, K. M.; Matolín, V.; Libuda, J. *J. Phys. Chem. C* **2016**, *120*, 9852–9862.
- (191) Wang, Y.-G.; Mei, D.; Glezakou, V.-A.; Li, J.; Rousseau, R. *Nat. Commun.* **2015**, *6*, 6511.
- (192) Aleksandrov, H. A.; Neyman, K. M.; Hadjiivanov, K. I.; Vayssilov, G. N. *Phys. Chem. Chem. Phys.* **2016**, *18*, 22108–22121.
- (193) Feynman, R. P. *J. Microelectromech. Syst.* **1992**, *1*, 60–66.